Role of Smart-Release Pigments in Preventing Corrosion Driven Cathodic Disbondment of Organically Coated Hot Dip Galvanised Steel

Journal of The Electrochemical Society, 2023 **170** 011502

Role of Smart-Release Pigments in Preventing Corrosion Driven Cathodic Disbondment of Organically Coated Hot Dip Galvanised Steel

P. Ansell, [z] L. Berry, J. McGettrick, J. Searle, N. Wint, H. N. McMurray, [*] and G. Williams

Materials Research Centre, College of Engineering, Swansea University, Bay Campus, Fabian Way, Crymlyn Burrows, Swansea SA1 8EN, United Kingdom

The role of smart-release corrosion inhibitive pigments in preventing cathodic delamination of organically coated hot-dip galvanized steel (HDG) is investigated. The pigments consisted of hydrotalcite (HT) exchanged with a range of inorganic and organic anionic species and were dispersed in a model PVB coating. A scanning Kelvin probe (SKP) technique was used to determine cathodic delamination rates, and the inhibition efficiencies obtained for inorganic ions increased in the order CO_3^{2-} < MoO_4^{2-} < NO_3^- < VO_4^{3-} < WO_4^{2-} < PO_4^{3-} < CrO_4^{2-}. The inhibition efficiencies for organic-based pigments increased in the order triazole <phenylphosphonate <trans-cinnamate <benzoate <salicylate <benzotriazole. The inhibition efficiency afforded by the best performing organic inhibitor, benzotriazole (BTA), rivalled that of HT containing stored chromate anions. Findings are consistent with HT-BTA acting to sequester anions from the underfilm electrolyte, releasing BTA^- which subsequently strongly adsorbs on the underfilm metal surface but can also form an insoluble Zn-BTA precipitate at the coating-defect boundary.
 [DOI: 10.1149/1945-7111/aca8d2]

Manuscript submitted August 22, 2022; revised manuscript received November 22, 2022. Published January 20, 2023. *This paper is part of the JES Focus Issue on Critical Factors in Localized Corrosion in Honor of Gerald Frankel.*

Organic multilayer-coated HDG is highly technologically important in the construction and automotive industries. However, when a coating defect completely penetrates the organic coating system, then electrolyte can reach the metal substrate resulting in coating failure. One such coating failure mechanism is corrosion-driven cathodic disbondment, which occurs on iron, steel,[1–7] and hot-dip galvanized steel[8–10] substrates. This corrosion phenomenon is characterized by the ingress of a thin electrolyte layer beneath the delaminated coating, which couples anodic metal dissolution at a penetrative defect to cathodic oxygen reduction occurring at the coating disbondment site.[2,11–16] An elevated alkaline environment at the principal cathode site causes coating de-adhesion and disbondment by the dissolution of oxide layers and hydrolysis of interfacial bonds.[2,11–16] The rate of organic coating failure can be significantly reduced by adding corrosion inhibitive pigments dispersed within an organic coating system's primer and pretreatment layers. The primer layer commonly contains a dispersion of corrosion inhibitors that can provide active corrosion protection in the case of penetrative coating defects.

The most effective and widely used corrosion inhibitors known to date are those based upon hexavalent chromate, e.g. strontium chromate ($SrCrO_4$).[17] However, hexavalent chromium is toxic,[18] carcinogenic[19] and prohibited under the Registration, Evaluation, Authorization and Restriction of Chemicals (REACH) directive.[20] This is particularly problematic when considering the sparingly soluble nature of such inhibitors, which means that they can dissolve in water and slowly leach out of the coating over time, limiting corrosion resistance and potentially leading to long-term environmental effects. It is therefore of great importance to develop environmentally friendly, Earth-abundant, and effective corrosion inhibitor pigments to replace those based on hexavalent chromate salts.

Current chrome-free corrosion inhibitor systems are based upon sparingly soluble phosphate such as calcium phosphate, zinc phospate and polyphospates.[21–23] Various studies have assessed the efficacy of phosphate as a corrosion inhibitor and shown that phosphate primarily offers anodic inhibition via a reaction with anodicly evoleved metal cations to form a protective insoluble precipitate.[24–30] However, phosphate has been identified as a critical raw materials in the European unions 2020 report; meaning that due to phosphates high demand in many key sectors phosphates are of high economic importance and high supply chain risk.[31]

A promising new technology designed to prevent the drawbacks of sparingly soluble salts, which utilizes encapsulated inhibitors species and may rival hexavalent chromate in corrosion protection, is based on "smart-release" corrosion inhibitor pigments.[32–36] Smart release inhibitors are characterized by their ability to release corrosion inhibitors under certain conditions, for example, a change in pH, electrochemical potential, or interaction with ionic species. In this latter case, smart release systems allow for active inhibition whereby species are only released when required upon exposure to an aqueous environment of sufficient ionic strength. Under such conditions, ion exchange will occur, releasing the corrosion inhibitor and sequestering corrosion stimulating ions.[37] One example of a smart release vehicle is hydrotalcite, a layered double hydroxide,[36,38–41] which has been shown to act as an effective release medium for both the protection of aluminium[32,42–45] and steel surfaces.[46–48] HT has the general formula $Mg_6Al_2CO_3(OH)_{16}{\cdot}4(H_2O)$ and is formed of positively charged layers of magnesium and aluminium. However, these cations can be substituted for other M^{2+} or M^{3+} metal ions, respectively. These positively charged layers are balanced by layers of weakly bound anions, typically carbonate.[49,50] The weakly bound anions can undergo ion exchange, allowing hydrotalcite to become a promising smart-release delivery system (see Fig. 1).[51]

HT pigments exchanged with various inorganic or organic inhibitors species have been shown to effectively inhibit filiform corrosion (FFC) on AA2024 aluminium alloy surfaces.[42–44] As-received HT containing exchangeable carbonate anions was shown to slow FFC propagation primarily by progressively removing aggressive chloride ions from the underfilm electrolyte.[42] However, HT pigment performance was significantly improved by replacing carbonate with highly efficient inhibitors, e.g. chromate.[42] A search of the literature reveals few studies on the effect of HT-based smart-release inhibitors on the rates of cathodic disbondment on HDG substrates. The literature on HT and other LDH has highlighted that the effectiveness of the smart release pigment is

*Electrochemical Society Member.
[z]E-mail: Philip.Ansell@swansea.ac.uk

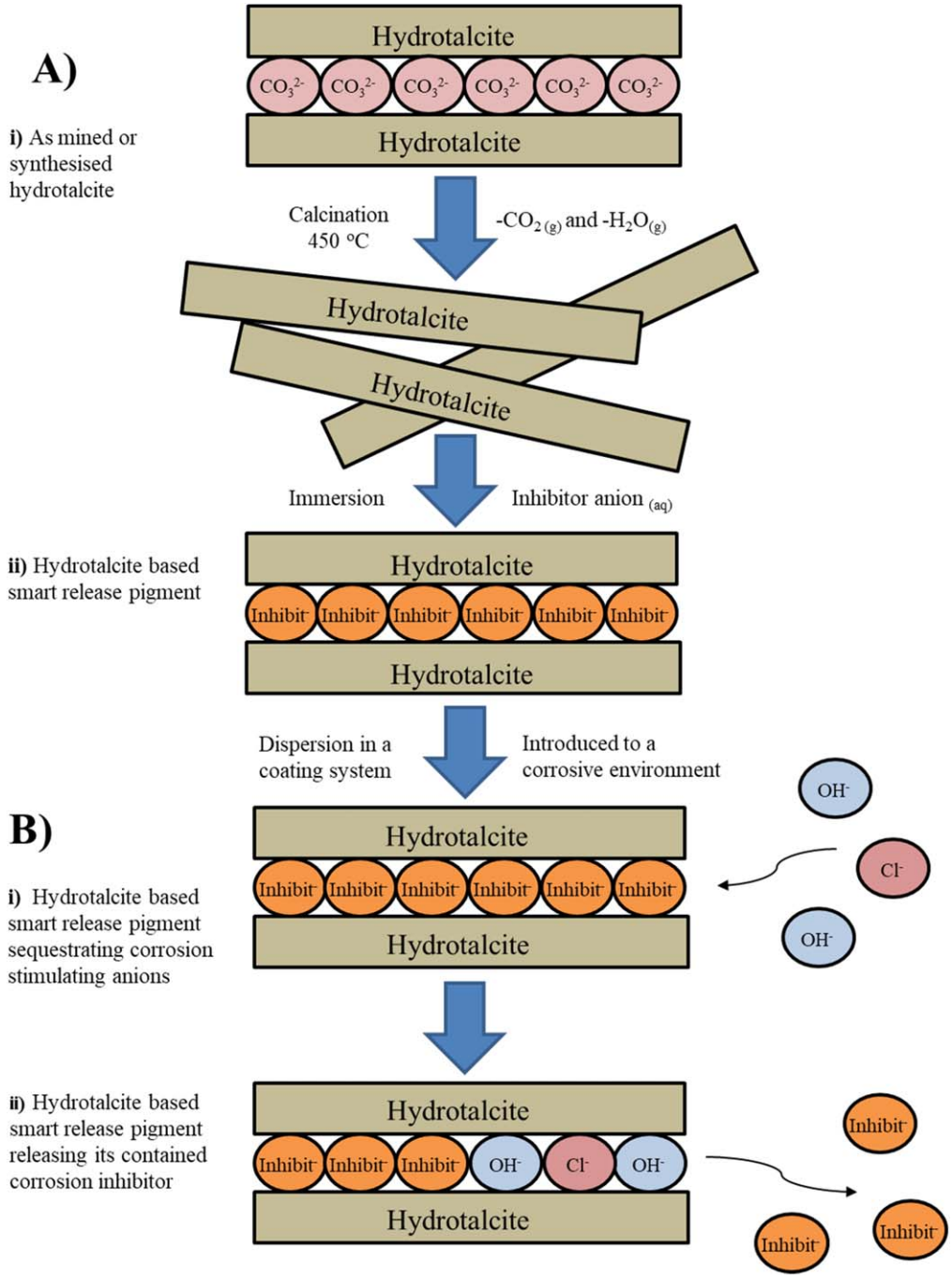

Figure 1. Schematic representation of hydrotalcite based smart release inhibitor preparation.

mainly dependent on the nature of the intercalated corrosion inhibitor.[38,40,52–55]

Having discussed the nature of the smart release vehicle used throughout this study, Hydrotalcite, the section below focuses on the various intercalated corrosion inhibitors. Many of the inhibitor ions selected for this study (CO_3^{2-}, NO_3^-, WO_4^{2-}, MoO_4^{2-}, PO_4^{3-}) have long been recognized as anodic corrosion inhibitors due to their ability to increases anodic polarisation by producing passivating films of sparingly soluble salts on the substrate surface. The films result from the reaction between metal ions produced from the anodic dissolution reaction and the inhibitor. Additionally, anodic inhibitors, as in the case of nitrate, molybdate and chromate, may act as oxidizing agents. Conversely, some of the inhibitor ions chosen for this study are cathodic or mixed corrosion inhibitors (CrO_4^{2-}, trans-cinnamate, benzoate, salicylate, benzotriazole). Cathodic inhibitors form insulating films, either by adsorption or by reacting with cathodically evolved hydroxide ions to form insoluble precipitates, which prevent electron transfer from the metal substrate at the cathode site. An alternate approach of cathodic inhibition suggested by Stratmann et al. involves removing free radical intermediates of the cathodic reaction using free radical scavengers (trans-cinnamate, benzoate, salicylate).[3] By doing so, cathodic inhibitors cause a negative shift in both E_{corr} and I_{corr}. A drawback of this study is that only anionic inhibitor species can be intercalated into HT and investigated. This excludes those cathodic inhibitors based on metal cations (e.g. Cr^{3+}) that provide inhibition by reacting with cathodically evolved hydroxide ions to form insoluble precipitates from this study.

Many of the inorganic ions selected have previously been successfully intercalated into hydrotalcite or LDHs and used as smart release inhibitor pigments on various substrates and various coating failure mechanisms. For example, HT- exchanged with decavanadate was using by Buchheit et al. in the pioneering work on HT as smart release inhibitors.[41] Furthermore, LDH exchanged with MoO_4^{2-} was previously used in a study conducted by Ogle et al.[55] in which the release kinetics of LDH's dispersed within organic coatings was systematically investigated. However, it is uncertain whether these inhibitor pigments will provide adequate corrosion protection against cathodic disbondment from HDG.

Finally, inhibitors were chosen that are known to perform effectively on HDG surfaces, namely benzotriazole (BTA), phosphate (PO_4^{3-})[56,57] and chromate (CrO_4^{2-}),[17,56] to evaluate their efficiency when stored within a smart-release HT pigment system.

The specific objective of this study is to assess the ability of a range of inorganic and organic anion exchanged-hydrotalcite systems to inhibit corrosion-driven cathodic disbondment of a model polyvinyl butyral (PVB) coating from HDG surfaces, where rates of cathodic disbondment were determined in situ using a scanning Kelvin probe (SKP). A further aim was to identify the most effective in-coating inorganic and organic anions and clarify the modes(s) by which inhibition of underfilm corrosion was achieved.

Materials and Methods

Materials.—Hot Dip Galvanised Steel (HDG) samples were provided by Tata steel UK and consisted of a 0.7 mm gauge mild steel substrate with a 20 μm zinc (containing approximately 0.15 wt % aluminium) layer. All chemicals, including hydrotalcite powder ($Mg_6Al_2(OH)_{16}CO_3{\cdot}4H_2O$), and Polyvinyl butyral-co-vinyl alcohol-co-vinyl acetate (PVB), molecular weight 70,000–100,000, were obtained from Sigma Aldrich Chemical Co. and were analytical grade purity.

Methods.— *Preparation of hydrotalcite (HT)-based smart release inhibitors.*—HT was used as an ion-exchange delivery device for the smart-release of various inhibitor anions. 10 g of HT was calcined at 450 °C for 3 h to remove the intercalated CO_3^{2-} and associated H_2O.[37,50,58] The calcined HT was then dispersed in 0.5 dm^{-3} of a 0.5 mol.dm^{-3} aqueous solution of the relevant inhibitor anion, whereupon the HT re-hydrates and intercalates the target anions within its layers. This process is illustrated in Fig. 1. Due to the limited solubility of some of the anions involved, the concentration of the solution was reduced, or a water-ethanol mixture was used as the solvent. The aqueous solution was prepared by boiling deionized water (DI) and then purging with nitrogen gas to remove any dissolved carbonate ions. The relevant inhibitor species (salts where possible) were then added to the treated DI. The solution pH was modified to the value of the inhibitor pK_a (by the dropwise addition of 2 mol.dm^{-3} NaOH solution) to ensure dissociation. The solution was stirred overnight to ensure maximum exchange. Once exchanged, the solution was centrifuged to separate the solid-smart-release-inhibitor pigment from the remaining solution. The excess solution was then poured away, and the smart release inhibitor pigment was washed by vigorously mixing with DI water. The solid-smart-release-inhibitor pigment was again separated using the centrifuge, and the excess water was removed. The previous washing steps were repeated 3 times to ensure the removal of any excess inhibitor or counterions. The washed pigment was then dried and milled for 1 h using a Retsch planetary ball mill at 350 rpm. The resultant powder was passed through a series of sieves to isolate a particle size of <20 μm to produce a fine pigment.[43]

Corrosion driven cathodic disbondment measurements.—The oxide was removed from the HDG surface using a 5 μm polishing alumina slurry. The HDG was washed with distilled water and ethanol to remove any contaminants, followed by drying with a hairdryer. HT smart release inhibitor pigments were added to the model 15.5% w/w PVB coatings according to Eq. 1 where PVF is pigment volume fraction, M_{PVB} and ρ_{PVB} are the mass and density (0.8 g cm^{-1}) of PVB, respectively, and M_{pt} and ρ_{pt} are the mass and density of the HT pigment (in g cm^{-1}).

$$PVF = \left(\frac{1 + M_{PVB}{\cdot}\rho_{pt}}{M_{pt}{\cdot}\rho_{PVB}} \right)^{-1} \quad [1]$$

The progress of cathodic delamination was monitored using a scanning Kelvin probe (SKP). Stratmann cells were prepared following a well-established methodology.[1–3] Two parallel strips of electrical tape were applied to the metal substrate, leaving a 2 cm $\times$ 5 cm area exposed. A 1.5 cm $\times$ 5 cm length of scotch™ tape was securely attached perpendicular to one exposed side. PVB was bar coated over the exposed HDG area and air-dried. The dry coating thickness, as determined by a micrometre screw gauge, was 30 μm. The scotch tape was cut and lifted to reveal a 2 cm $\times$ 1.5 cm model defect, around which noncorrosive silicone rubber was applied to form a convenient well, or reservoir. Delamination was initiated by adding 1–2 ml of electrolyte to the model defect. For the purpose of providing a highly aggressive accelerated test conditions the electrolyte used was 0.86 mol.dm^{-3} $NaCl_{(aq)}$ at pH 7. All delamination experiments were carried out at 20 °C and a constant relative humidity of 96% (maintained via an isopiestic equilibrium with a 0.86 mol.dm^{-3} $NaCl_{(aq)}$ solution contained within the environmental chamber).

The SKP technique is the main non-perturbing procedure used to map the electrochemical activity of local corrosion sites beneath intact organic coatings and thin electrolyte layers. The design, operation and calibration of the SKP are discussed exhaustively elsewhere.[1,2,17] Briefly, the potential measured by the Kelvin probe is calibrated to standard electrode potentials by measuring a series of known redox couples (e.g. Ag/Ag^+, Cu/Cu^{2+}, Fe/Fe^{2+} and Zn/Zn^{2+}) and verified against the potentials measured by a potentiostat (Solartron 1280). SKP experiments were carried out within an enclosed environmental chamber, excluding electrostatic and electromagnetic noise while maintaining a controlled environment with constant gas composition and relative humidity. The Kelvin probe consisted of a 125 μm diameter 99.99% gold wire and acted as a reference probe relative to the sample under investigation. The SKP reference probe was scanned at a distance of 100 μm over the sample surface along a 12 mm line normal to and adjacent with the defect coating boundary. Scans were conducted immediately after adding the electrolyte to the artificial model defect and at 1 hr intervals thereafter. Twenty E_{corr} data points were recorded per mm. Probe vibration was achieved by connecting the probe to an audio speaker via a glass rod. The probes oscillation frequency was maintained at 280 Hz using a lock-in amplifier and a vibrating drive amplifier, and peak-to-peak amplitude was confirmed as 40 μm by using a strobe light and a travelling microscope.

Electrochemical measurements.—The electrochemical experiments were performed using a Gamry Interface 1010 potentiostat in conjunction with a 3-electrode arrangement comprising a saturated calomel reference electrode (SCE) and a Pt foil counter electrode. The working electrode consisted of a 0.95 cm^2 circular exposed area of HDG. All experiments were carried out in 0.86 mol.dm^{-3} $NaCl_{(aq)}$ solutions to provide comparable conditions to those used for the SKP experiments. Before starting the potentiodynamic polarisation experiments the samples were immersed in the electrolyte and left at open cuircuit potential for five minutes to allow the samples to equilibriate and for the potential to stabilize. For the potentiodynamic polarisation experiments, seperate samples were polarised 0.3 V vs SHE away from the open circuit potential, positively in the case of the anodic branch or negatively in the case of the cathodic branch. A scan rate of 0.1667 mV s^{-1} was used for all experiments. Each experiment was repeated three repeats three times to ensure reproducibility of the results.

Scanning electron microscopy and energy dispersive spectroscopy.—Images were obtained using a Hitachi S-4800 Field Emission Gun Scanning Electron Microscope (FEG SEM) with Oxford instruments Silicon Drift X-Max EDS Detector and Inca EDS software. For all SEM imaging an operating voltage and current of 15 kV and 20 μA was used respectively. Prior to imaging, HDG coupons were covered in PTFE with 1 cm^2 or bare metal exposed and immersed in the relevant electrolyte for one week.

Results and Discussion

A preliminary delamination experiment was carried out using unpigmented PVB on an HDG substrate to establish baseline kinetics. The distinctive E_{corr} vs delamination plots obtained can be seen in Fig. 2.

After the sample reached an equilibrium in humid air (96% relative humidity), a relatively high and constant E_{corr} of ca. −0.4 V vs standard hydrogen electrode (SHE) was observed over the intact coating (E_{intact}), which is comparable to the value recorded for uncoated HDG samples under the same conditions.[17,59] The E_{intact} represents the open circuit potential of a substrate, in this case, zinc, when coated with an adherent, nonconducting polymer before the ingress of the bulk electrolyte. The E_{intact} for a nonconducting polymer/metal interface is the result of the electrochemical situation, which is determined by reactions 2 and 3 where the rate of the oxygen reduction reaction (ORR) is high due to rapid oxygen diffusion through the highly oxygen-permeable polymer and a slow anodic dissolution reaction due to lack of bulk electrolyte.[9,15,60,61] The intact potential will be shifted to more positive values if the rate of the anodic dissolution reaction (3) is slowed. This can be caused by a dense oxide scale, a surface treatment or by active pigmentation of the polymer.[61]

$$O_2 + 2H_2O + 4e^- \rightarrow 4OH^- \quad [2]$$

$$Zn_{(s)} \rightarrow Zn^{2+} + 2e^- \quad [3]$$

Initiation of delamination of the unpigmented model coating was observed an hour after adding the electrolyte (0.86 $mol.dm^{-3}$ $NaCl_{(aq)}$) to the bare metal defect adjacent to the PVB coated region. Figure 2 shows a schematic representation of the cathodic disbondment cell, along with the corresponding distinctive time-dependent E_{corr} vs delamination distance (X_{del}) profiles obtained at hourly intervals by in situ SKP analysis.[17]

A sharp potential drop from the intact potential −0.4 V to ca. −0.7 V vs SHE characterizes the location of the delamination front. The potential drop has been attributed to the balance between a faster rate of ORR (2) relative to zinc dissolution (3). The potential difference between the E_{intact} and the defect regions establishes a galvanic cell where a local cathode forms at the delamination front and the local anode at the defect. A progressive negative shift in the E_{corr} of the defect/coating boundary directly adjacent to the delamination zone is typically observed over time. This negative

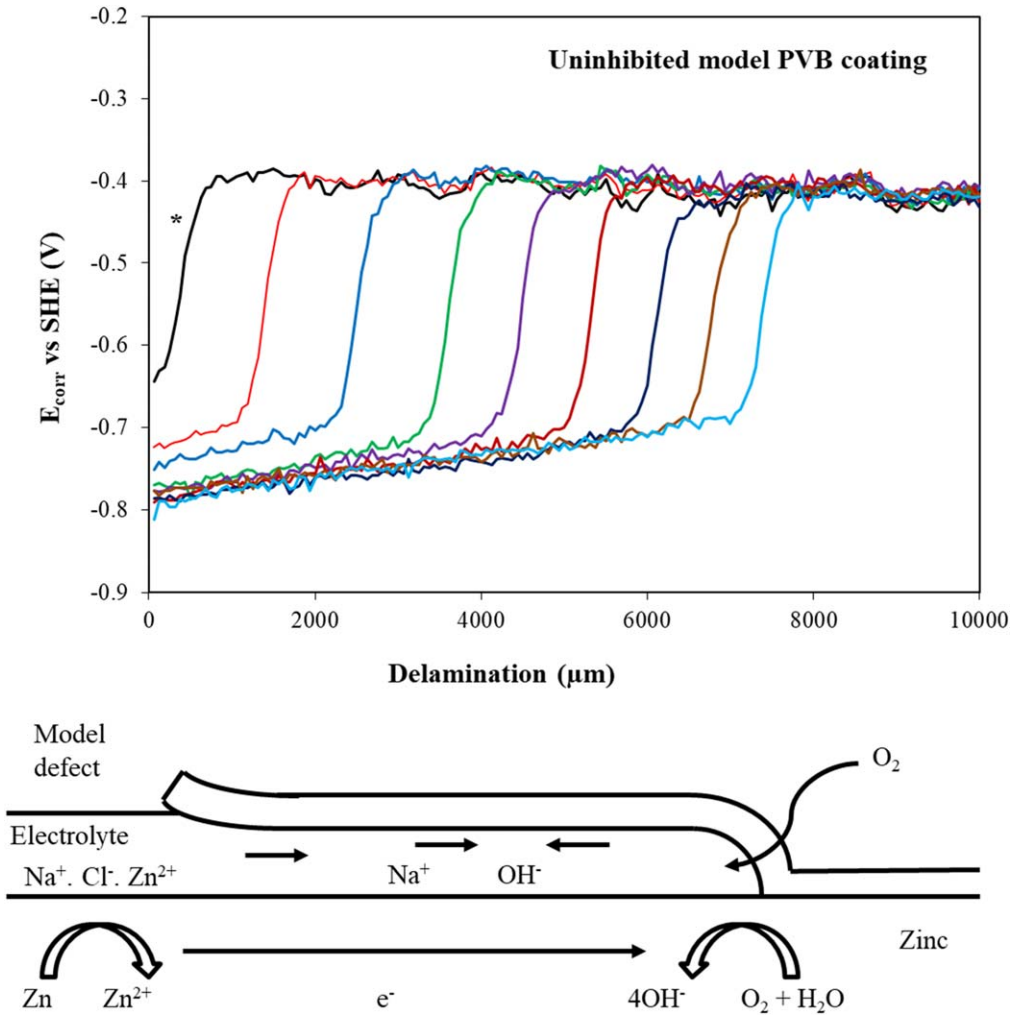

Figure 2. (above) Plots of the time-dependent E_{corr} vs delamination distance profiles recorded for PVB on HDG steel substrates shown at hour intervals, commencing at 1 h post initiation* and ending after 9 h. Delamination was initiated with 0.86 M NaCl. (below) Corresponding schematic representation of the corrosion driven cathodic disbondment cell.

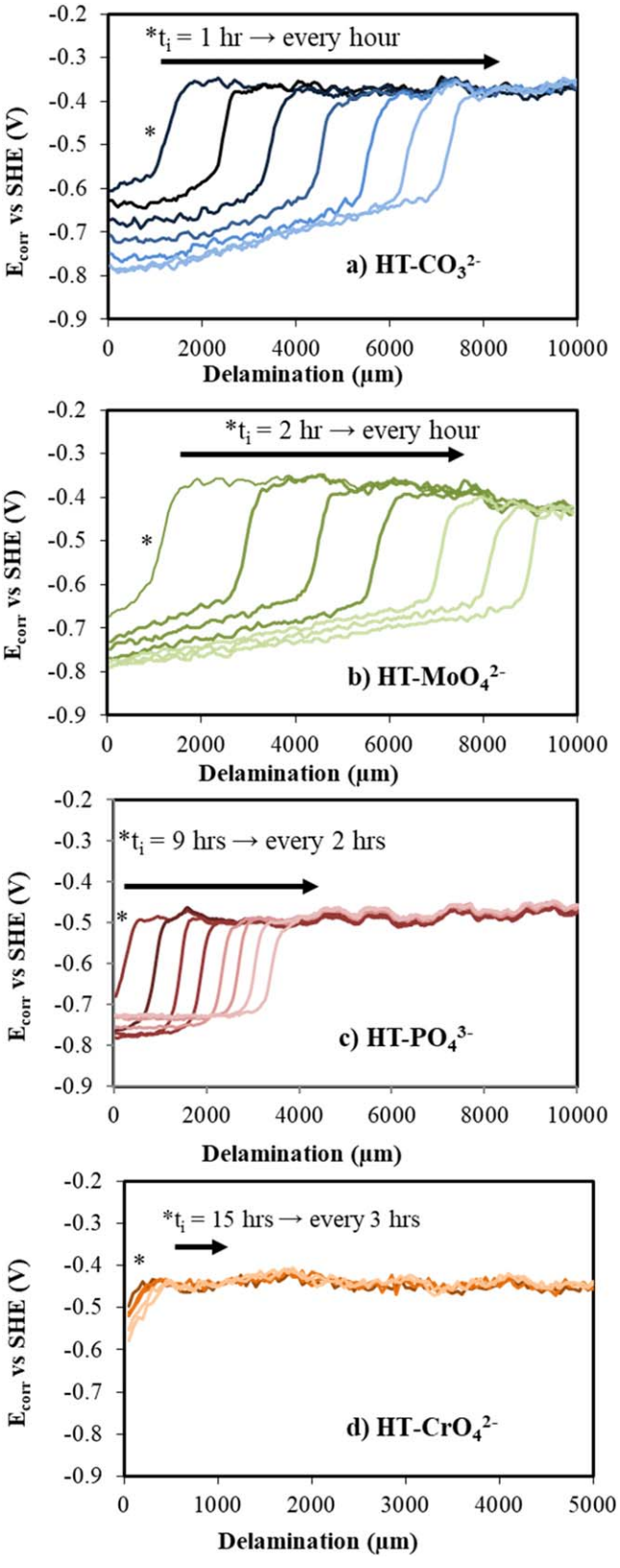

Figure 3. Plots of the time-dependent E_{corr} vs delamination distance profiles recorded for PVB containing 0.1 PVF (a) HT – CO_3^{2-} (b) HT – MoO_4^{2-} (c) HT-PO_4^{3-} (d) HT – CrO_4^{2-} on HDG steel. Delamination was initiated (t_i) with 0.86 M NaCl.

potential shift to the final potential typical of a free corroding zinc electrode in chloride containing electrolyte is thought to result from the dissolution of anodically inhibitive protective hydroxide and oxide layers.[8,9] Anodic dissolution (3) occurs at the penetrative coating defect, where bare zinc is exposed. The raised underfilm alkalinity caused by reaction 2 results in the dissolution of amphoteric zinc oxide at the substrate-coating boundary leading to coating de-adhesion.[62] The dissolution of zinc oxide and zinc hydroxide surface layers produce soluble aqueous bizincate ($HZnO_2^-$) and zincate (ZnO_2^-) species according to reactions 4 and 5.

$$Zn(OH)_{2\,(S)} \leftrightarrow HZnO_{2\,(aq)}^{-} + H_{(aq)}^{+} \quad [4]$$

$$Zn(OH)_{2\,(S)} \leftrightarrow ZnO_{2\,(aq)}^{2-} + 2H_{(aq)}^{+} \quad [5]$$

Furthermore, the elevated alkalinity can also activate the bare zinc surface in the delaminated zone, allowing for direct oxidation to bizincate ($HZnO_2^-$) as shown in reaction 6.[63]

$$Zn_{\,(S)} + 2H_2O \leftrightarrow HZnO_{2\,(aq)}^{-} + 3H_{(aq)}^{+} + 2e^{-} \quad [6]$$

Between the areas of the delamination front and the model defect, there is a smaller drop in the potential of ca 0.1 V vs SHE to a potential of ca. −0.8 V vs SHE. This gradual potential drop has been attributed to an ionic current passing through the thin layer of underfilm aqueous electrolyte, which ingresses between the HDG surface and the disbonded coating. This links the net underfilm cathode at the disbondment front with the net anodic located at the bare metal defect. Typically, the ionic current and delamination rate are limited by the migrational mass transport of cations (e.g. Na^+) from the initiating electrolyte (in the model defect) to the delamination front. However, there are cases reported in the literature, such as under the effect of a corrosion inhibitor, where interfacial electron transfer associated with cathodic ORR becomes rate limiting and produces a change in the cathodic disbondment kinetics.[64–66]

Corrosion inhibitor pigments based on inorganic anion exchanged hydrotalcite.—A preliminary screening exercise was conducted to determine the relative efficiency of the various inorganic anion-exchanged pigments at a PVF of 0.1. Figure 3 shows a selection of SKP-derived E_{corr} versus distance profiles obtained for various inorganic anion-bearing HT pigments, ranging from the least to the most effective types. The E_{corr} vs X_{del} profiles obtained for a HT – CO_3^{2-} and HT-MoO_4^{2-} pigments (Figs. 3a and 3b) are similar to the unpigmented coating given previously in Fig. 2, with little change observed in the values of E_{corr} in both the intact (ca. −0.4 V vs SHE) and defect adjacent (ca. −0.8 V vs SHE) regions of the delamination cell. In addition, the extent of time-dependent delamination (X_{del}), as signified by the sharp drop in E_{corr}, appears to be largely unaffected by the presence of the pigments. The notable difference seems to be in the respective steepness of the E_{corr} versus X_{del} plots gradients observed in the vicinity of the delaminated region, which links the defect region (at $\times = 0$) to the disbondment front (region I). For an unpigmented PVB coating, a dE_{corr}/dX_{del} gradient of ca. 1.5×10^{-5} V μm^{-1} is observed at holding times of >4 h, while the presence of the HT – CO_3^{2-} and HT-MoO_4^{2-} pigments causes the dE_{corr}/dX_{del} gradient to increase to a value of 2.8×10^{-5} and 4.0×10^{-5} V μm^{-1}, respectively. The E_{corr} of the delaminated region adjacent to the model defect is significantly more positive at $t = 0$ in the case of HT – CO_3^{2-} containing PVB (ca. −0.6 V vs SHE) relative to the unpigmented control (ca. −0.65 V vs SHE). Furthermore, the presence of both pigments delayed the onset of delamination by 1 and 2 h for HT – CO_3^{2-} and HT-MoO_4^{2-} respectively.

Unsurprisingly, E_{corr} vs X_{del} profiles obtained for the addition of 0.1 PVF HT – PO_4^{3-} showed some significant difference relative to the unpigmented control. A positive shift in the potential of the intact coating and a progressive, positive rise in the E_{corr} values (−0.8 V to

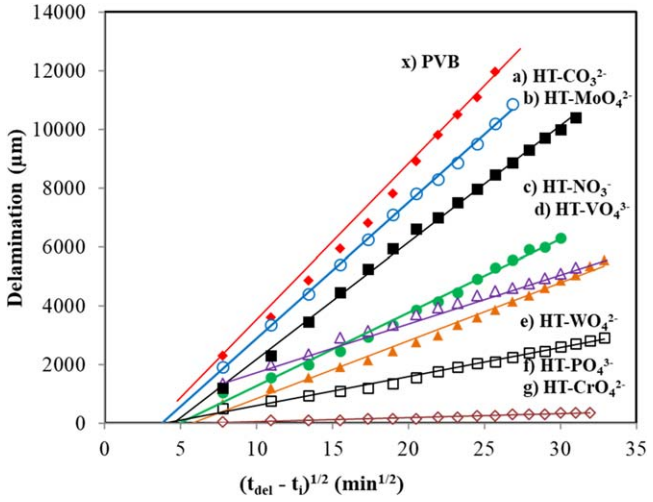

Figure 4. Plots of delamination distance (X_{del}) as a function of $(t_{del}\text{-}t_i)^{1/2}$ for PVB films containing 0.1 PVF of HT exchanged with various inorganic corrosion inhibitors.

Table I. Values of parabolic rate constants (K_{del}), percentage rate change at a PVF of 0.1 for inorganic inhibitors exchanged HT within a PVB model coating.

	K_{del} (μm min$^{1/2}$)	ΔK_{del} (%)
PVB	544.12 ± 15.24	0%
HT-CO_3^{2-}	462.85 ± 12.96	15%
HT-MoO_4^{2-}	398.01 ± 11.14	27%
HT-NO_3^-	249.5 ± 6.99	54%
HT-WO_4^{2-}	197.31 ± 5.52	64%
HT-VO_4^{3-}	165.52 ± 4.63	70%
HT-PO_4^{3-}	98.83 ± 2.78	82%
HT − CrO_4^{2-}	13.35 ± 0.37	97%

−0.74 V vs SHE) within the delamination zone were observed. Furthermore, HT − PO_4^{3-} dispersed within the PVB coating caused a 9 h delay in the onset of delamination.

The E_{corr} vs X_{del} plot obtained for additions of HT − CrO_4^{2-} resemble those obtained for the unpigmented case, albeit concentrated closer to $X_{del} = 0$ and only progressing after a 15 h delay in initiation time. The only other observable difference appears to be a negative shift in the E_{intact}. Although, due to the low X_{del}, the delaminated zone was not resolved.

Having measured the E_{corr} vs X_{del} profiles for each inhibitor system and unpigmented PVB, the delamination rates can be determined. This has been traditionally done using the sharp potential drop from the intact potential to the delaminated region as a semiempirical measure of the position of the delamination front. Therefore, using the E_{corr} vs X_{del} plots, the distance from which the delamination front has moved (X_{del}) can be determined for any time (t_{del}) after adding the initiating electrolyte (t_i). It has previously been shown that during cathodic disbondment, the rate-limiting migrational mass transport of cations gives rise to parabolic delamination kinetics and is characterized by Eq. 7. Under these conditions X_{del} is related to t_{del} by the following expression, where K_{del} is the delamination rate constant.[8,17]

$$X_{del} = K_{del}(t_{del} - t_i)^{1/2} \quad [7]$$

Therefore, by plotting time-dependent X_{del} values as a function of $(t_{del}\text{-}t_i)^{1/2}$ for each smart release inhibitor pigment as well as those obtained 0.1 PVF of HT intercalated with nitrate, ortho-vanadate, tungstate and unpigmented PVB, the K_{del} can be plotted and used as a measure of the efficiency of each inhibitor (in Fig. 4). The primary source of error when determining K_{del} is the semiempirical measure of the position of the delamination front. Therefore, K_{del} errors were measure from multiple repeats of the control experiment, the cathodic disbondment of PVB from HDG. From the resulting E_{corr} vs X_{del} profile, the time-dependent X_{del} values were plotted as a function of $(t_{del}\text{-}t_i)^{1/2}$ and the K_{del} obtained by linear regression. The errors are plus or minus one standard deviation on the mean of the multiple control experiments. Under the conditions employed here, the efficiency of the inhibitive anion type increases in the order $CO_3^{2-} < MoO_4^{2-} < NO_3^- < VO_4^{3-} < WO_4^{2-} < PO_4^{3-} < CrO_4^{2-}$. Values of K_{del}, measured from the slopes of the plots given in Fig. 4, are summarised in Table I, along with percentage changes of K_{del} relative to the unpigmented PVB control coating.

The lowest K_{del} were measured were for the model PVB coating contained 0.1 PVF of HT − CrO_4^{2-} and HT − PO_4^{3-}, 13.35 ± 0.37 and 98.83 ± 2.78 μm min$^{1/2}$ respectively, which is a 97% and 82% reduction relative to the control coating (544.12 ± 15.24 μm min$^{1/2}$).

As previously stated, the rate-limiting step for cathodic disbondment is typically the migrational mass transport of cations, giving rise to parabolic delamination kinetics and characterized by Eq. 7. For all smart release inhibitor pigment dispersed coatings tested and the unpigmented PVB control, parabolic delamination kinetics appear to be observed (which give rise to a linear relationship when X_{del} is plotted as a function of $(t_{del}\text{-}t_i)^{1/2}$). However, the delamination kinetics must be interpreted cautiously when the delamination distance is small and has not reached completion. In such cases, the initial rates may not be representative, and deviation to higher-order kinetics may become apparent with additional data points. The initial rate of coating delamination is used for comparison purposes.

For both HT − CO_3^{2-} and HT-MoO_4^{2-} there was little change in the potential values obtained relative to the unpigmented PVB control (Fig. 2). However, there was a change in the gradient of the dE_{corr}/dX_{del} slopes, which joined the cathodic delamination front to the anodic defect. Stratmann et al. attributed this potential gradient to the ohmic potential drop caused by the ionic current of cations migrating from the local anode within the model defect to the cathodic delamination front.[45] An increased dE_{corr}/dX_{del} gradient within the underfilm delaminated region has previously been interpreted in the literature as an increase in the resistance of the underfilm electrolyte.[9,67,68] Let us now consider the inhibition of HT-MoO_4^2. Unexchanged MoO_4^{2-} is well known for being an effective corrosion inhibitor, forming Mo-rich protective layers on HDG, although not in high alkaline pH such as those encountered at the cathode front.[55,69–71] These findings may account for the increase dE_{corr}/dX_{del} gradient and the delay in delamination initiation. This pH dependence may have contributed to the ineffective inhibition under the conditions employed here with HT-MoO_4^{2-} producing a 27% reduction in rate relative to the unpigmented PVB control. This finding, while preliminary, implies the importance of effective inhibition of corrosion within the area of the delamination front.

In the case of HT − CO_3^{2-} (see Fig. 3a), a small increase in the E_{corr} of the underfilm electrolyte was observed. According to mixed potential theory, this slight positive shift in the presence of HT − CO_3^{2-} is consistent with a net anodic inhibition. This and the previous finding is consistent with the literature; It has previously been shown that carbonate (CO_3^{2-}) ions can provide modest corrosion inhibition of HDG substrates by the formation sparing soluble zinc carbonate layer ($K_{sp} = 1.5 \times 10^{-10}$).[72] The inability of HT − CO_3^{2-} to significantly inhibit cathodic delamination appears at odds with previously published results, where it was shown to act effectively in slowing rates of FFC on aluminium surfaces.[42–44] In these previous studies, the corrosion inhibition was attributed to the ability of the HT to sequester chloride ions from the electrolyte within the filament head and with the associated release of carbonate ions further moderating the underfilm pH.[42,44] In the case of cathodic

disbondment, during which chloride is excluded from the underfilm electrolyte, the ion exchange process will involve sequestering underfilm OH^-, produced by reaction (4), the presence of which ultimately causes coating disbondment. These seemingly contradictory results show that the removal of OH^- by HT in the quantities measured here has a negligible effect on the rate of disbondment.

Whatever the inhibitory effect HT − CO_3^{2-} offers, it would seem insufficient in and of itself to induce any significant influence on the extent of delamination. For HT − CO_3^{2-} only a slight 16% reduction in the rate of cathodic disbondment was measured relative to an unpigmented PVB coating. The results obtained here have implications for understanding the baseline rates of inhibition of as received of HT (HT − CO_3^{2-}) and demonstrate that the as-received pigment does little to reduce the rates of cathodic disbondment.

Unsurprisingly, the addition of 0.1 PVF HT − PO_4^{3-} resulted in some notable changes in the E_{corr} vs delamination distance profiles (see Fig. 3c). The effectiveness and mechanism of PO_4^{3-} based corrosion inhibitors are well known and discussed elsewhere.[73–75] In this study, HT − PO_4^{3-} significantly slowed the disbondment rate by 82% reduction relative to unpigmented PVB. Surprisingly the presence of HT − PO_4^{3-} caused a ca. 0.15 V vs SHE negative shift in E_{intact} of the PVB coated HDG surface compared to the unpigmented case. The negative shift in the E_{intact} in the presence of the inhibitor is consistent with net cathodic inhibition. However, it must be noted as there is an absence of an aqueous electrolyte, non-faradic electrostatic contributions could influence the shift if E_{intact}.[76–78]

Also, a progressive rise in E_{corr} (−0.8 V to −0.74 V vs SHE) within the underfilm delaminated zone was observed. Previously, such observed changes in E_{corr} have been ascribed to the adsorption of inhibitive anions onto the oxide covered metal surface present at the metal-polymer interface.[43,44] This result is consistent with many studies, which states that PO_4^{3-} primarily offers anodic inhibition via the formation of an insoluble $Zn_3(PO_4)_{2(s)}$ precipitate ($K_{sp} = 9 \times 10^{-33}$ mol^5 dm^{-15}).[25–30]

Finally, CrO_4^{2-} released from HT was shown to be highly efficient at slowing rates of cathodic disbondment. In the presence of HT − CrO_4^{2-} pigment (Fig. 5d), the rate of coating disbondment within 30 h of the initiation of corrosion was negligible, with a 97% reduction relative to unpigmented PVB coating, which was in line with previous observations.[17] One unanticipated finding was that HT-CrO_4^{2-} achieved a superior level of inhibition than Cr(VI) with a significantly lower quantity of inhibitor added to the coating under the same conditions.[17,42]

The significant implication of these findings is that HT is working effectively as a delivery mechanism under the conditions employed here and, when combined with a suitable intercalated species, an inhibitor of corrosion driven cathodic disbondment. Furthermore, that the smart release inhibitor pigments effectiveness is highly dependent on the intercalated inhibitor.

From Fig. 4, it is apparent that the nature of the anion strongly influences the delamination rate. The finding is supported by the result obtained in the case of as-received and unexchanged HT (comprising of exchangeable carbonate anions), for which only a marginal reduction in coating failure rate compared with unpigmented PVB was observed. Under the conditions employed here, the efficiency of the inhibitive anion type increases in the order CO_3^{2-} < MoO_4^{2-} < NO_3^- < VO_4^{3-} < WO_4^{2-} < PO_4^{3-} < CrO_4^{2-}. Parabolic kinetics would suggest that even under circumstances where the in-coating inhibitor appears to work highly effectively (e.g. Figure 4, PO_4^{3-} and CrO_4^{2-} respectively), cation migration seems to persist as the rate-limiting step.

A closer investigation of the performance of HT − CO_3^{2-}, HT-MoO_4^{2-}, Ht-PO_4^{2-}, and HT − CrO_4^{2-} was carried out by systematically varying the PVF within the model PVB coating. The resulting K_{del} were extracted and plotted in Figs. 5a–5d, which all show a systematically increasing the PVF produces a progressive decrease in delamination rate. Parabolic kinetics persist for all pigments and for all PVF tested. HT-CrO_4^{2-} at the highest PVF tested, 0.2 PVF, delivers no detectable delamination over a 24 hr period, although only a small benefit is observed when increasing the PVF from 0.1 to the maximum value of 0.2 employed in this study.

The underlying mechanism of CrO_4^{2-} inhibition is discussed in detail elsewhere.[17] Briefly, it was proposed that the significant factor in decreasing delamination involved the replacement of under-film O_2 reduction (via Eq. 2) by a self-limiting CrO_4^{2-} reduction process, represented by reaction (8).

$$CrO_4^{2-}{}_{(aq)} + 5H_2O_{(l)} + 3e^- \rightleftharpoons Cr(OH)_{3(s)} + 5OH^-_{(aq)} \quad [8]$$

Hydrolysis of Cr(III) at elevated pH produces a solid hydroxide, which rapidly blocks off further cathodic activity on the original underfilm site of ORR (K_{sp} $Cr(OH)_3 = 5.8 \times 10^{-13}$ mol^2 dm^{-6}).[79]

However, the current study found that a superior level of inhibition of cathodic disbondment from HDG was observed in the presence of 0.1 PVF HT − CrO_4^{2-} relative to 0.049 PVF of $SrCrO_4$ with a significantly lower quantity Cr(IV) ions added to the coating.[24] The use of HT as a smart release delivery device could be a factor in the improved efficiency. There are several significant differences between the modes by which smart release based HT − CrO_4^{2-} and sparingly soluble based $SrCrO_4$ could inhibit corrosion. The differences in these modes of corrosion inhibition are indicative of the smart release delivery device. For example, HT − CrO_4^{2-} can release CrO_4^{2-} ions directly into the area of the local cathode at the delamination front via ion exchange with OH^- ions. In contrast, previous studies have shown that sparingly soluble based Cr(IV) ions are electrostatically excluded from this region.[24] Another significant difference in the modes of inhibition mentioned in a prior study is the importance of fast inhibitor release kinetics on the inhibition of cathodic disbondment.[59] It is plausible the release kinetic of HT − CrO_4^{2-} is more rapid than those based on sparing soluble salts under the conditions studied here (high pH and a small volume of electrolyte).[80–83]

Corrosion inhibitor pigments based on organic-anion-exchanged HT.—Of the inorganic inhibitors investigated, only chromate and phosphate ions provided a significant slowing in cathodic disbondment. Both chromate and phosphate ions form the basis of the current state-of-the-art anti-corrosion pigment technology based on sparingly soluble salts. Therefore, the findings of the previous section serve only to provide additional support regarding why such technologies are in everyday use. Thus, to identify novel, environmentally friendly and effective alternatives, an investigation of corrosion inhibitive pigments based on HT exchanged with various organic inhibitors was undertaken. The same rationale for inhibitor selection was employed from the previous section. Briefly, the organic inhibitors must be anionic in nature, be known or anticipated to provide corrosion inhibition or previously have been intercalated into HT or another layered double hydroxide. The organic inhibitors intercalated into HT in this study were triazole (HT-TZ^-), trancinnamate (HT-TC^-), phenylphosphonate (HT-PPH^-), benzoate (HT-BZ^-), salicylate (HT-SAL^-) and benzotriazole (HT-BTA^-). The smart release inhibitors effectiveness and efficiency at reducing rates of cathodic disbondment of a PVB model coating containing a 0.1 PVF inhibitor loading were evaluated using in situ SKP analysis. The E_{corr} vs X_{del} profiles obtained for each smart release pigment is presented in Figs. 6a–6f.

The E_{corr} vs X_{del} profiles obtained for HT- organic-based pigments showed significant differences relative to unpigmented PVB. An increase in E_{intact} relative to an unpigmented control coating was observed for coatings containing 0.1 PVF of HT-PPH^-, HT-SAL^-, HT-BTA^- and HT-BZ^-. The most significant rise in E_{intact} was observed for HT-PPH^- and HT-SAL^- which showed a ca. 0.2 V and a 0.15 V vs SHE positive shift relative to the

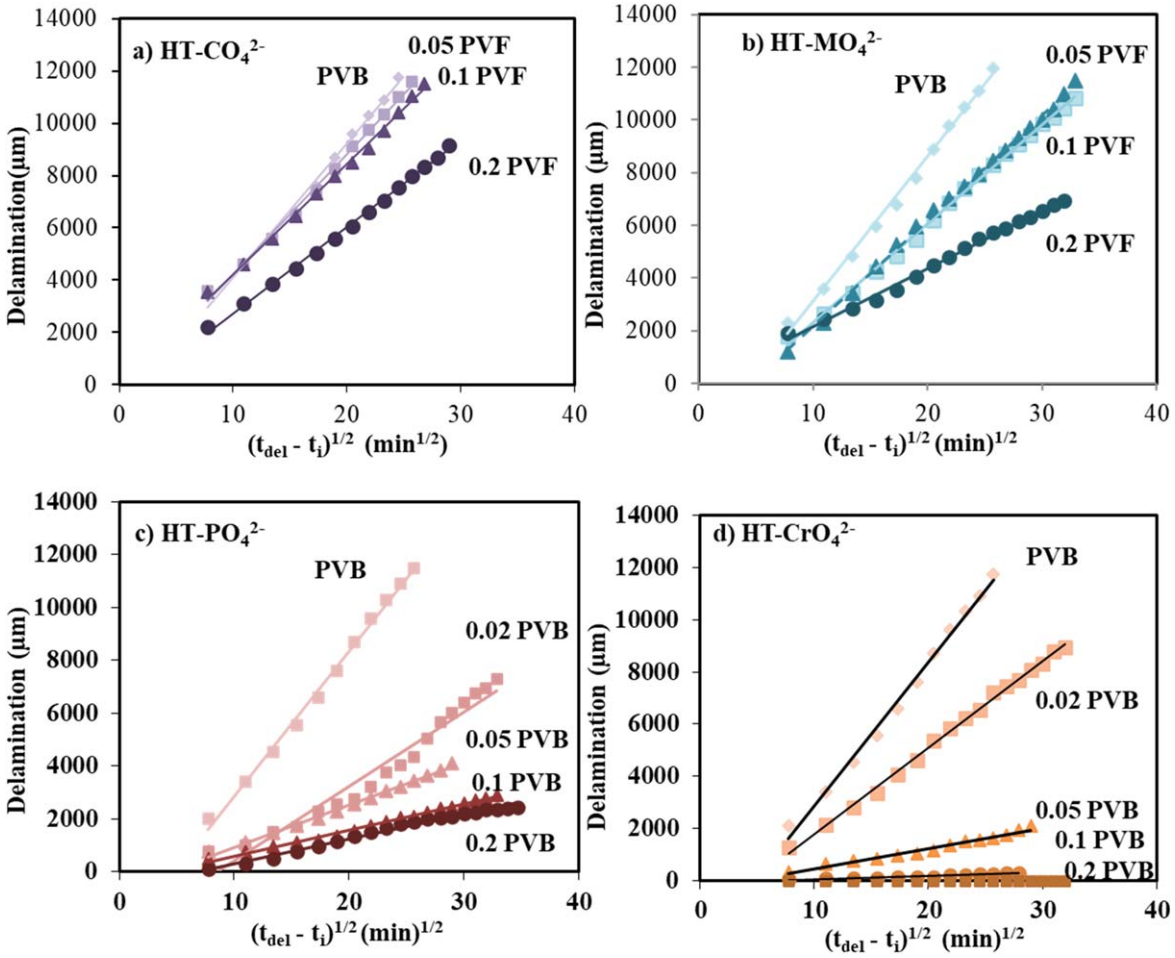

Figure 5. Plots of delamination distance (X_{del}) as a function of $(t_{del}\text{-}t_i)^{1/2}$ for PVB films containing various PVF of (a) HT $-$ CO_3^{2-} (b) HT-MoO_4^{2-} (c) Ht-PO_4^{2-}, and (d) HT $-$ CrO_4^{2-}.

unpigmented control and HT-BTA^- and HT-BZ^- showing smaller positive shifts of ca. 0.1 V and ca. 0.05 V vs SHE, respectively (see Fig. 6).

The addition of HT-organic inhibitors also seems produce some changes to the potentials measured within the underfilm delaminated region. A time-dependent progressive-positive potential shift in the underfilm delamination region was observed for HT-TC^-, HT-BZ^-, HT-SAL^- and HT- BTA^-. This positive potential shift is most pronounced for the phenolate based inhibitors and increases in the order HT-SAL^- < HT-BZ^- < HT-TC^- with the most considerable shift observed some ca. 0.2 V vs SHE. For HT-TC^- a significant decrease in E_{corr} at the defect-coating boundary (at $X_{del} = 0$) was also observed.

In the case of HT-TZ^- containing coatings, a complete loss of coating adhesion in the region behind the delamination front was observed, causing the PVB/HT composite coating to lift away from the substrate. This loss of coating adhesion caused the coating to come into close proximity to the SKP probe, producing instrumental artifacts which have been excluded for the sake of clarity. Furthermore, a time-dependent progressive negative shift in the E_{corr} within the delaminated region was observed.

In the cases of HT-TC^- and HT-PPH^-, the gradient of the dE_{corr}/dX_{del} slope observed between the cathodic front and model defect are significantly steeper ca. 7.0×10^{-5} and 8.6×10^{-5} V μm^{-1} than in the unpigmented case ca. 1.5×10^{-5} V μm^{-1}. Interestingly, the E_{corr} vs X_{del} profiles obtained for the delamination of PVB containing HT-SAL^- are dramatically different to the unpigmented control. In the delaminated zone adjacent to the model defect, the potential is more positive (ca. -0.7 V vs SHE) than the unpigmented control (ca. -0.8 V vs SHE) and slowly increases over time.

Using the E_{corr} vs X_{del} profiles for each smart release inhibitor system studied in this section (Figs. 6a–6f) and unpigmented PVB (Fig. 2), the K_{del} can be determined and used as a measure of the efficiency of each inhibitor. This is achieved by measuring the time-dependent progression of the delamination front, X_{del}, and plotting it as a function of $(t_{del}\text{-}t_i)^{1/2}$. Under the conditions employed here, the efficiency of smart release inhibitors increases in the following order: HT-TZ^- < HT-PPH^- < HT-TC^- < HT-BZ^- < HT-SAL^- < HT-BTA^-. Values of K_{del}, obtained from the gradients given in Fig. 7, are summarised in Table II, along with values for the percentage reduction in K_{del} relative to an unpigmented PVB coating. The greatest reduction in the K_{del} was observed for those PVB coatings containing 0.1 PVF of HT-SAL^- and HT-BTA^- with a K_{del} of 62.352 ± 1.75 and 12.46 ± 0.35 $\mu m\ min^{1/2}$ respectively or a ca. 89% and 98% reduction relative to an unpigmented PVB coating. Parabolic delamination kinetics appear to be observed (which give rise to a linear relationship when X_{del} is plotted as a function of $(t_{del}\text{-}t_i)^{1/2}$ for all HT inhibitors studied except for HT-BZ^-, HT-SAL^- and HT-BTA^- which appears to deviate to a higher order. This may be indicative of a change in the rate-limiting step of cathodic disbondment from the typically migrational mass transport of cations to the cathodic ORR.

Of the organic anion–based pigments evaluated, the addition of HT-triazole resulted in the lowest inhibition efficiency, causing complete coating disbondment within the 12 mm SKP scanned area in less than 11 h and therefore increases cathodic disbondment relative to unpigmented PVB (Fig. 6a). Triazole is cited as a

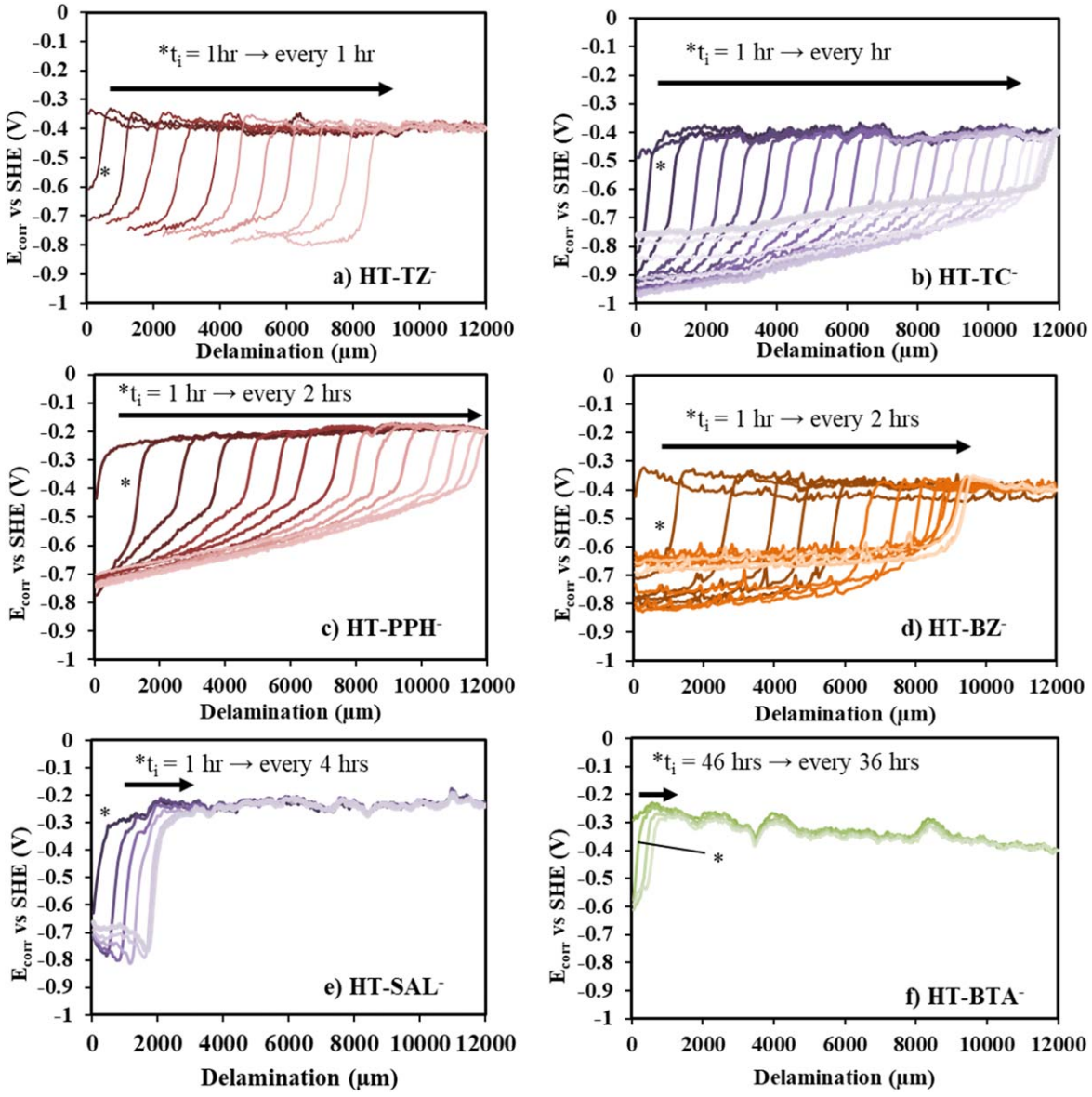

Figure 6. Plots of the time-dependent E_{corr} vs delamination distance profiles recorded for PVB containing 0.1 PVF of (a) HT-TZ^- (b) HT-TC^- (c) HT-PPH^- (d) HT-BZ^- (e) HT-SAL^-, and (f) HT-BTA^- on HDG steel. Delamination was initiated (t_i) with 0.86 M NaCl.

corrosion inhibitor on aluminium,[84] copper[85,86] and iron[87] substrates typically under immersion conditions and is thought to offer corrosion inhibition by forming a thin chemisorbed film on the metal surface.[85] In addition, it is also known to act as an anodic inhibitor, reacting with metal ions to form a protective passivating layer.[88] However, no evidence of these modes of inhibition have been observed under the specific conditions employed here, and the presence of triazole appears to accelerate rather than inhibit cathodic delamination from HDG.

0.1 PVF of phenyl phosphonate (PPH^-) exchanged HT dispersed PVB coating reduced cathodic disbondment from HDG by ca. 38%. The E_{corr} vs X_{del} profiles (Fig. 6c) show the dE_{corr}/dX_{del} gradient measured within the delaminated zone is significantly steeper, ca. 8.6×10^{-5} V μm^{-1}, than in the unpigmented case (ca. 1.5×10^{-5} V μm^{-1}). Similar results were observed in the case of the delamination 0.1 PVF of HT-TC^-, HT-CO_3^{2-} and HT-MoO_4^{2-} dispersed PVB coatings from HDG. Previous studies have suggested that an increase in the steepness of this dE_{corr}/dX_{del} gradient may indicate an increase in the resistance of the underfilm electrolyte. This result is seemingly contrary to the previous work of Glover et al., who conducted a series of experiments whereby phenyl phosphonic acid (H_2PP) was added directly to a PVB model coating and determined resultant cathodic delamination rates as a function of H_2PP content using in situ SKP.[63]The acid liberated by the dissociation of H_2PP was shown to etch the HDG surface, liberating zinc ions and buffering the underfilm pH and forming an insoluble film of zinc monophenylphoshonate, blocking electron transfer and the underfilm cathodic reduction reaction.[89] However, when introduced in the form of an HT-PPH^- pigment, the important acid etch step is not present, and hence the observed reduction in K_{del} is significantly lower than that of in-coating phenyl phosphonic acid directly added to PVB. In the case of a PVB coating containing 0.1 PVF HT-PPH^- the most significant increase in E_{intact} ca. 0.2 V vs SHE relative to the control coating was observed, as well as a negative shift in the underfilm delamination zone. This increase in E_{intact} and E_{corr} of the delamination zone is consistent with predominately anodic inhibition within these regions. The mode of inhibition of smart release HT-PPH^- relative to H_2PP are likely similar; however, it appears that without the critical acid etch step, the reduction in the K_{del} is significantly lower.

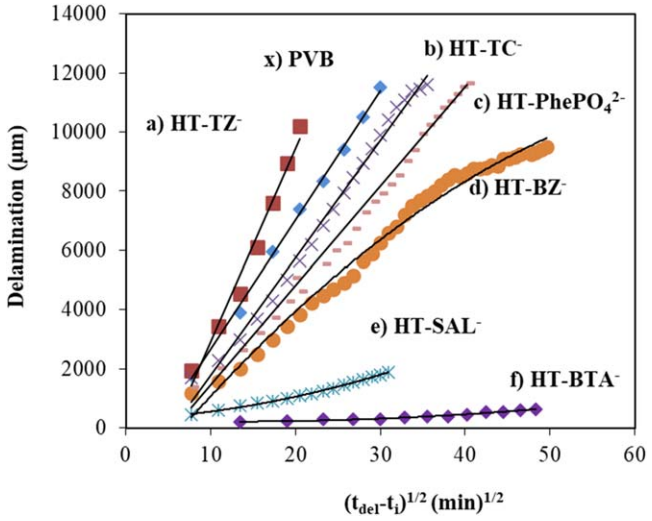

Figure 7. Plots of delamination distance (X_{del}) as a function of $(t_{del}\text{-}t_i)^{1/2}$ for PVB films containing 0.1 PVF of HT exchanged with various organic corrosion inhibitors.

Table II. parabolic rate constant (K_{del}) at a PVF of 0.1 for organic inhibitor exchanged HT within a PVB model coating and percentage change in delamination rate (ΔK_{del}) relative to an unpigmented PVB coating.

	K_{del} (μm min$^{1/2}$)	ΔK_{del} (%)
HT-TZ$^-$	437.07 ± 12.24	−22%
PVB	544.12 ± 15.24	0%
HT-TC$^-$	397.57 ± 11.13	27%
HT-PP$^-$	335.56 ± 9.40	38%
HT-BZ$^-$	216.43 ± 6.06	60%
HT-SAL$^-$	62.352 ± 1.75	89%
HT-BTA$^-$	12.46 ± 0.35	98%

The E_{corr} vs X_{del} plots obtained for HT-TZ$^-$, HT-BZ$^-$ and HT-SAL$^-$ dispersed PVB coatings share several similarities, as shown in Figs. 6b, 6d and 6e. This is unsurprising as these inhibitor ions contain the same aromatic and carboxylate functionalities.

Each of the aromatic carboxylate-based inhibitors cause a time-dependent progressive, positive E_{corr} shift within the delaminated coating region, which increases with time. In the case of 0.1 PVF of HT-BZ$^-$ and HT-SAL$^-$ dispersed PVB coatings, an increase in E_{intact} of ca. 0.5 V and ca. 0.15 V vs SHE respectively was observed relative to unpigmented PVB coating. Interestingly, HT-SAL$^-$ dispersions were observed to cause some striking changes in E_{corr} vs X_{del} profiles relative to the other inhibitors and unpigmented PVB.

When the time-dependent X_{del} data for the delamination of 0.1 PVF HT- aromatic carboxylate-based inhibitors dispersed PVB coating is plotted as a function of $(t_{del}\text{-}t_i)^{1/2}$, shown in Fig. 7, K_{del} extracted from the gradient can be used as a measure of inhibitor effectiveness. Considering Fig. 7, it appears HT-SAL$^-$, provides a much stronger level of inhibition than the other carboxylate-based inhibitors and correspondingly reduced K_{del} considerably (89%) relative to the PVB control experiment and when compared with the HT-TC$^-$ (27%) and HT-BZ$^-$ (60%).

Closer inspection of Fig. 7 shows that for the delamination of PVB coatings containing 0.1 PVF of HT-SAL$^-$ and HT-BZ$^-$, a deviation to higher-order delamination kinetics appears to be observed. This is caused by a shift in the rate-determining step of cathodic disbondment. Typically, the rate-determining step of cathodic disbondment is the migration of cations from the defect to the delamination front. Under mass transport control, with increasing time and distance of delamination, parabolic delamination kinetics become established (or linear kinetics when plotted against $(t_{del}\text{-}t_i)^{1/2}$). Previous studies have shown that a change in delamination kinetics is indicative of a change in the rate-determining step from a migrational mass transport of cations to electron transfer to the ORR within the cathodic disbondment front. Furthermore, this change in delamination rate can result from cathodic inhibitors forming protective layers within the cathode, reducing electron transfer to the ORR.

Earlier studies suggest all the aromatic carboxylate-based inhibitors investigated can act as cathodic inhibitors by forming a thin absorbed layer on the metal surface, reducing oxygen diffusion to the metal substrate surface and suppressing the cathodic reaction.[30,90,91] Consistent with the literature, a negative shift in E_{corr} adjacent to the cathodic front relative to the unpigmented control was observed in the case of HT-SAL$^-$ containing coatings.

Another important finding was that all HT- aromatic carboxylate-based inhibitors cause a time-dependent progressive, positive shift in E_{corr} within the delaminated coating region. Furthermore, coatings containing 0.1 PVF of HT-BZ$^-$ and HT-SAL$^-$ an increase in E_{intact} of ca. 0.5 V and ca. 0.15 V vs SHE respectively was observed relative to unpigmented PVB coating.

These results suggest that these inhibitors provide predominately anodic inhibition within these regions, which is consistent with the literature. Previous studies state that HT-BZ$^-$ and HT-TC$^-$ readily react with zinc ions through carboxylate functionalities forming insoluble precipitates.[92–94] Although zinc salicylate is soluble in water, the reaction between salicylic acid and ZnO results in the formation of insoluble plastic-like masses of 2:1 Zn(salicylate) and 1:1 Zn(salicylate) salts.[95–97]

A surprising result is that relative to the control coating, for HT-SAL$^-$ containing coatings, a more positive potential value is observed adjacent to the model defect (ca. −0.7 V vs SHE) and a more negative potential is observed in the region which trails the disbondment front (ca. −0.8 V vs SHE). As mentioned before, the positive potential shift adjacent to the defect is consistent with anodic inhibition. Whereas, the literature states that such a negative shift in E_{corr} is maybe consistent with cathodic inhibition, but also that an E_{corr} of ca. −0.8 V vs SHE is compatible with a freely corroding zinc electrode.

In this respect, the E_{corr} vs X_{del} profiles' shape resembles those obtained for filiform-like corrosion, where anodic undermining is the principal organic coating de-adhesion mechanism.[43,44] However, after removing the specimen under investigation from the SKP chamber after 24 h, there was no visual evidence of the presence of copious corrosion product marking the site of disbondment, which would be expected had a polarity reversal of the delamination cell occurred, leading to chloride ion ingress. However, it could be argued that this hypothesis is unlikely as in the case of chloride ion ingress, increased ion exchange with the dispersed HT-SAL$^-$ pigment would cause increased release of inhibitor ions.

Salicylic acid, salicylate and other phenolic carboxylates are commonly recognized as free radical scavengers which undergo progressive hydroxylation, dimerization and polymerisation.[98–100] Stratmann et al. showed that the ORR free radical intermediates ($O_2^{-\bullet}$ and $OH^\bullet$) caused significant oxidative destruction of the metal/polymer interface and was an important factor in cathodic disbondment. Furthermore, corrosion-driven cathodic disbondment has been achieved by dispersing free radical scavengers within various polymer coating by Sorensen et al..[101] It is consistent with the literature that salicylate could be interfering with the cathodic reaction by removing free radical intermediates necessary for the destruction of the metal/polymer interface[3]. The ultimate product of such reactions would be a poly-SAL film that has been reported to cause electrode passivation or fouling[102–104] and used to protect metals.[105] Whether such a protective polymeric film is present and the exact mode of inhibition offered by HT-SAL$^-$ is still unknown, and further studies are therefore suggested. It appears that in the case

of cathodic disbondment of PVB coatings from HDG that HT-phenolate inhibits reduce the rates of delamination via a mixed inhibitory mode. However, for the most effective HT-phenolate inhibitors investigated, there is evidence to suggest cathodic inhibition is an important factor.

By far the most effective corrosion inhibitor in reducing the rate of cathodic disbondment of PVB from HDG was HT-BTA^-. Initiation of delamination was not observed over a 24 h period for PVF of 0.1. Experiments were extended up to 4 days to determine if cathodic disbondment eventually occurred. Initiation of delamination only occurred 40 h after the addition of the initiating electrolyte, whereas in the case of an unpigmented PVB coating, it can be detected after 1 h. The E_{corr} vs X_{del} profiles in Fig. 6f obtained after the onset of delamination exhibit some significant differences to those shown in Fig. 2 for uninhibited PVB. Although the progress of the delamination front was measurable, the reduction in K_{del} relative to the PVB control was considerably higher (98%) than all other HT based pigment systems and similar to that obtained for $HT-CrO_4^{2-}$ containing coatings (97%). The presence of the HT-BTA^- within the PVB coating appears to positively shift both the potential of the intact coating ca. +0.15 V and the delaminated underfilm region ca. +0.2 V relative to unpigmented PVB coating. This result is in accordance with a predominantly anodic inhibitor within these regions. Similar E_{corr} vs X_{del} profiles have been observed for amberlite based smart releases inhibitors exchanged with cationic $BTAH_2^+$ under the same conditions.[106] Previous studies have shown that BTA acts as an anodic inhibitor when dosed into chloride containing aqueous solution by reacting with zinc ions formed during anodic dissolution and forming an insoluble precipitate.[106]

When considering the time-dependent X_{del} data plotted versus $(t_{del}\text{-}t_i)^{1/2}$ for HT-BTA containing PVB coating and the resulting K_{del}, it appears a deviation in rate kinetics is observed relative to unpigmented PVB. Therefore, it seems that a switch in the rate-determining step of cathodic disbondment has occurred. For unpigmented PVB, the rate-determining step has been shown to be the migrational mass transport of cations from the defect to the delamination front. The deviation in delamination kinetics has previously been attributed to a change in the rate-determining step of cathodic disbondment to interfacial electron transfer to the ORR.[107]

Due to the efficiency of HT-BTA^- at reducing the rate of cathodic disbondment, an in-depth investigation of this particular pigment's performance was carried out by systematically varying the PVF dispersed within the model PVB coating. The resulting time-dependent X_{del} is plotted as a function of $t_{del}\text{-}t_i$ instead of $(t_{del}\text{-}t_i)^{1/2}$ used prominently throughout this study for ease of comparison, and the data is shown in Fig. 8. Increasing HT-BTA^- PVF from 0.005 to 0.20 led to a progressive and significant decrease in the rate of delamination. From this data, we can see that the unpigmented PVB control coating gives rise to parabolic delamination kinetics indicative of mass transport control. However, for HT-BTA^- containing coatings, in all cases, it appears a switch in the delamination kinetics is observed relative to the control coating. Previous research has established that the presence of cathodic inhibitors may cause such a marked switch in delamination kinetics by reducing the rate of the interfacial ORR.

These experiments have confirmed that HT is an effective smart release delivery system, with its inhibition efficiency being highly dependent on the intercalated inhibitor anion type. The results appear to show that the most efficient HT smart release inhibitors investigated seem to do so via causing a change in the rate-determining step of cathodic disbondment from migrational mass transport to the to one of interfacial electron transfer involving underfilm ORR.

Evaluation of benzotriazole-substrate interaction.—HT-BTA^- has been shown to be an effective inhibitor of HDG corrosion. The addition of HT-BTA^- delays the onset of delamination and once initiated, slows the rate of delamination, and causes a change in the kinetics. Based on these results, it could be hypothesized that BTA acts to inhibit corrosion-driven cathodic disbondment via mixed inhibition. Therefore, the extent to which and the mechanism by which HT-BTA^- provides corrosion protection will be investigated, explored and discussed.

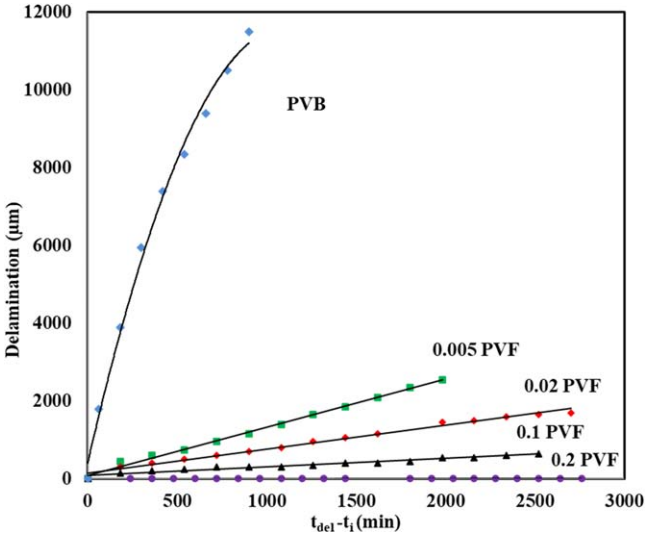

Figure 8. Plots of delamination distance (X_{del}) as a function of $(t_{del}\text{-}t_i)^{1/2}$ for PVB films containing various PVF of HT-BTA^-.

The change in delamination kinetics observed in Figs. 7 and 8 is indicative of cathodic inhibition. It is plausible that once exchanged, BTA^- adsorbs at the metal electrolyte interface and inhibits the cathodic ORR (2) and electron transfer reactions within the underfilm delamination region and cathodic delamination front.

From Fig. 6f a progressive, positive shift in potential was observed within the region of the delamination zone and the intact coating. In accordance with mixed potential theory, such observations have previously been ascribed to anodic inhibition. It is possible, therefore, that once exchanged, anionic BTA (see reactions 9 and 10) may react with anodically evolved zinc ions to form an insoluble precipitate, which inhibits the anodic dissolution reaction (3), within the region of model defect.

$$BTAH_2^+ \leftrightarrow BTAH + H^+ pK_a \approx 1.1 \quad [9]$$

$$BTAH \leftrightarrow BTA^- + H^+ \; pK_a = 8.2 \quad [10]$$

The increase in E_{intact} observed may result from reactions of atmospheric oxygen or Bronstead acids or bases with the coating and metal (oxide) surface.[17,78,106] A change in E_{intact} has previously been ascribed to the effect of inhibitor release from a smart release pigment before the addition of the initiating and interaction with the bulk electrolyte.[106] Ion exchange may occur between cathodically produced hydroxide ions and the small proportion of HT-BTA^- dispersed throughout the model coating at the metal coating interface. Once released, the inhibitor reacts with the zinc surface, causing passivation. In the region of the undelaminated coating, in the absence of bulk electrolyte anodic inhibition reaction of BTA^- with anodically evolved zinc ions is improbable. Anion BTA may passivate the zinc surface in a similar manner to that proposed previously by Birblus et al. It was postulated that the mechanism of inhibition of BTA anions on a Magnesium alloy (in wt%: Mg-12.1Zn-3.5Al-0.3Mn-0.1Ca-0.0029 Fe) was to act as a nucleating agent which activates the formation of a densely packed passivating $Mg(OH)_2$ layer.[108] However, the amount of HT-BTA^- present at the polymer-metal interface in the undelaminated coating region available to undergo exchange is assumed to be small, due to the absence

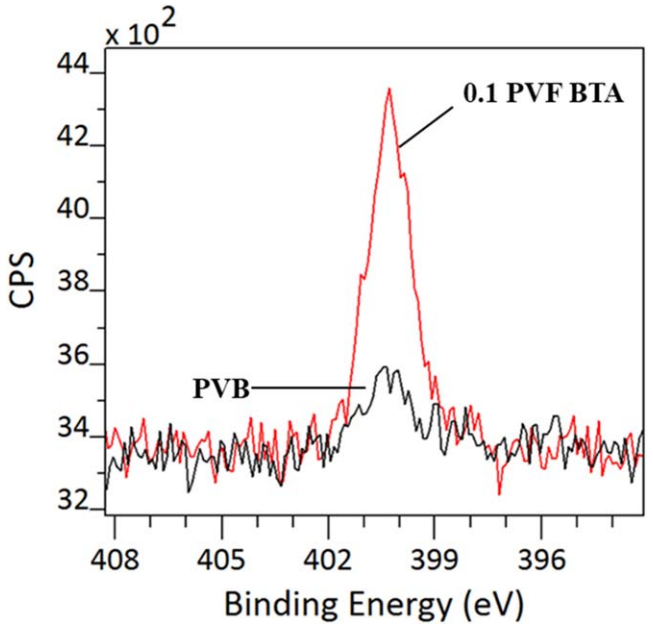

Figure 9. Showing the obtained XPS spectra of the Stratmann cells model defect region after the SKP experiments using PVB coatings with and without 0.1 PVF dispersed HT-BTA^{-}.

of bulk electrolyte, and therefore the overall contribution to the inhibition of corrosion-driven cathodic disbondment would be negligible. From these results it can be inferred that HT-BTA^{-} provides predominantly cathodic inhibition in the underfilm delamination zone and the cathodic delamination front. Furthermore, that HT-BTA^{-} produces anodic inhibition by complexing with anodically produced zinc ions in the region of the model defect. Therefore, it is likely that anodic and cathodic inhibitor mechanisms are responsible for the considerable combined effect on the inhibition of cathodic disbondment.

Anodic inhibition resulting from the reaction of BTA^{-} with zinc ions is thought to be a significant factor in the overall corrosion inhibition mechanism. A white precipitate was observed in the model defect of the Stratmann cell following delamination of coatings containing HT-BTA^{-}. It is possible that once anionic BTA^{-} is released from the HT, it migrates into the model defect where it may react with zinc ions (formed during the primary anodic reaction (5)) to form an insoluble zinc/BTA salt or complex according to reactions 11 and 12.

$$Zn^{2+}_{(aq)} + 2BTA^{-}_{(aq)} \rightarrow Zn(BTA)_{2(s)} \quad [11]$$

$$Zn^{2+}_{(aq)} + BTA^{-}_{(aq)} \rightarrow [ZnBTA]_{n\,(s)} \quad [12]$$

X-ray photoelectron spectroscopy (XPS) analysis, shown in Fig. 9, of the white precipitate showed the presence of an N1s peak (400 eV binding energy). No nitrogen peak was detected for the unpigmented PVB control. These XPS results suggest that BTA^{-} is present within the model defect. This result would seem to be at odds with Richards et al. findings where the author, investigating the effects of a cationic BTA (9) containing pigment on the rates of cathodic disbondment of PVB from HDG and found there was no evidence of cationic BTA within the model defect.[106] However, this finding is unsurprising when considering that cationic BTA would be electrostatically excluded from the model defect due to the anodic dissolution of zinc ions (3).

Further surface analysis was required to determine the nature of the insoluble precipitate formed. The samples were characterized using SEM and EDX were split into three groups; the first HDG sample was left untreated, the second sample was immersed in

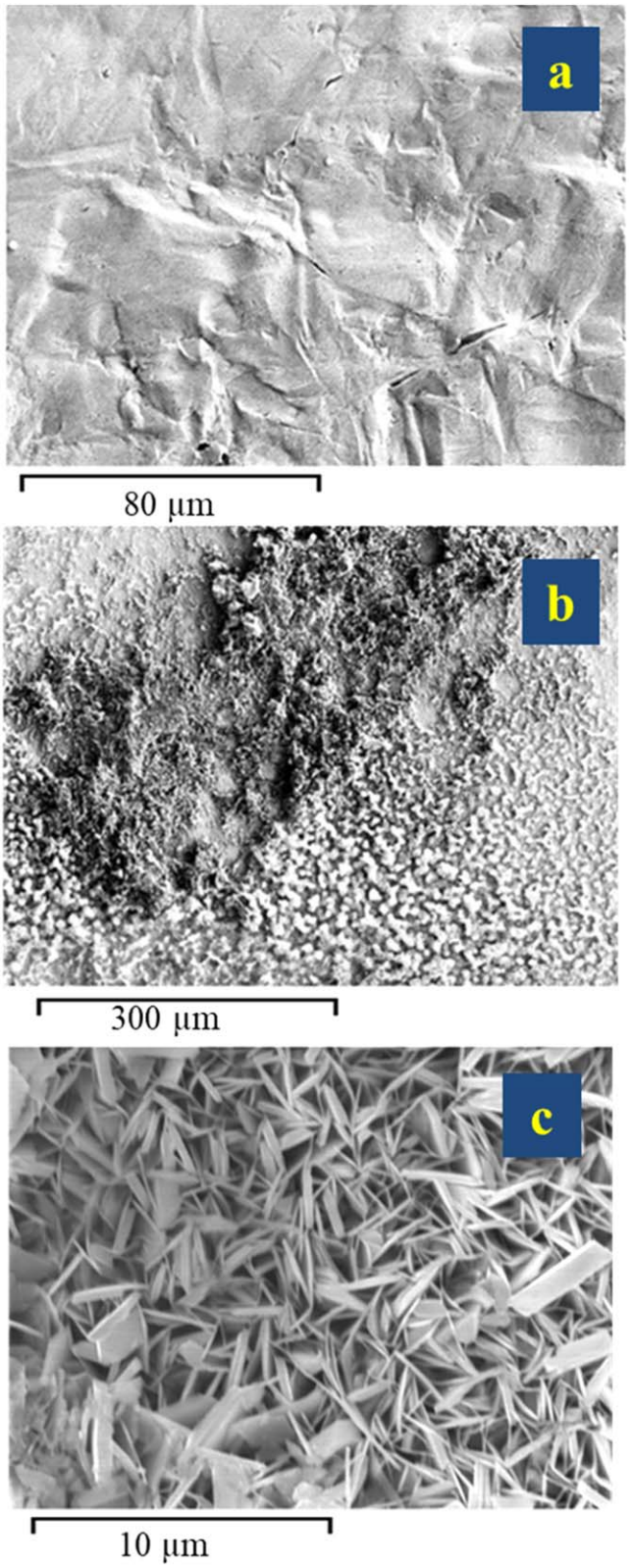

Figure 10. (a) SEM images of untreated HDG. (b) HDG after immersion in 0.86 mol.dm^{-3} NaCl$_{(aq)}$ solutions and (c) with the addition of 0.1 mol.dm^{-3} BTA for one week.

0.86 M NaCl for one week, and the third was submerged in both 0.86 mol.dm^{-3} NaCl and 0.1 mol.dm^{-3} BTA$_{(aq)}$ again, for one week. The first HDG sample, which was left unsubmerged as a control (Fig. 10a) showed a typical smooth surface. The second sample,

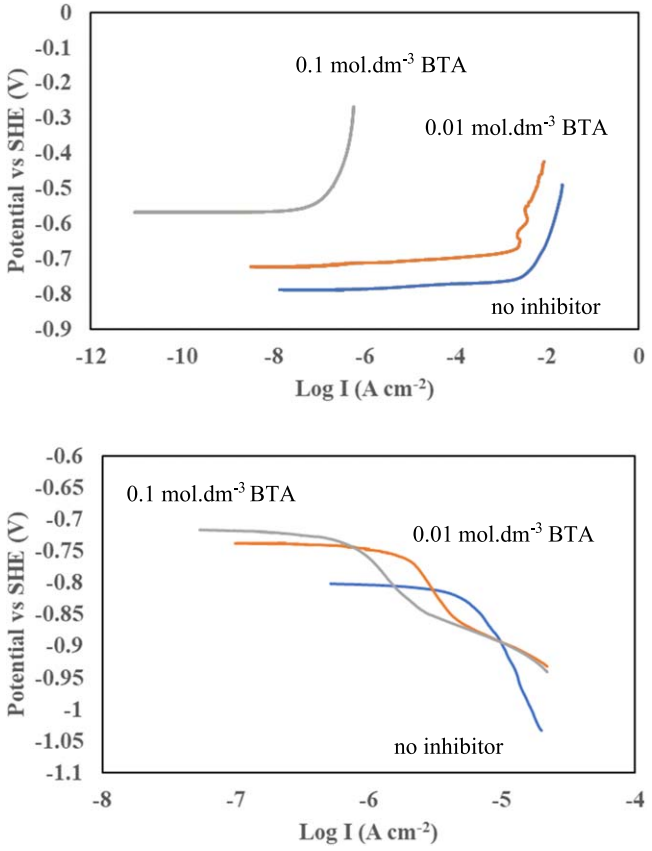

Figure 11. Potentiodynamic polarization curves for (a) anodic and (b) cathodic branches for HDG immersed in 0.86 mol.dm^{-3} $NaCl_{(aq)}$ solutions (blue, no inhibitor) with and without the addition of 0.01 mol.dm^{-3} (orange) and 0.1 mol.dm^{-3} (gray) of BTA. The potentiodynamic scan rate was 0.1667 V s^{-1}.

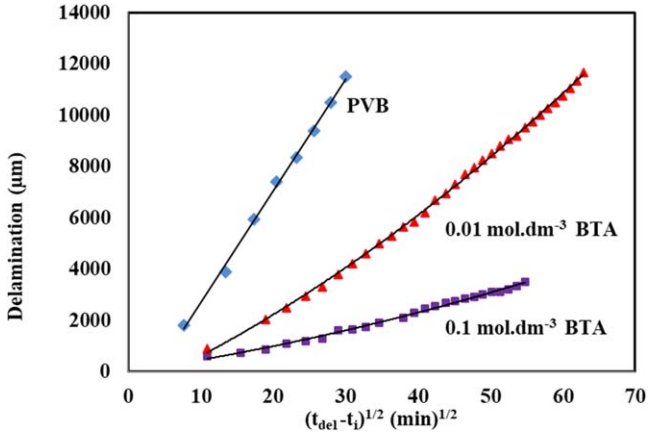

Figure 12. Plots of delamination distance (X_{del}) as a function of $(t_{del}-t_i)^{1/2}$ for PVB from HDG with different concentrations of BTA added to the initiating electrolyte.

which was left un-inhibited in salt solution, showed a highly roughened and corroded surface (Fig. 10b). The third sample, submerged in both BTA and NaCl solution, showed a platelet like surface morphology (Fig. 10c). These results further support the presence of an insoluble Zn:$BTA_{n(s)}$ precipitate, providing anodic inhibition.

The extent to which anodic or cathodic modes of inhibition contribute to the observed inhibition of the rate of cathodic disbondment from HDG was investigated via a series of potentiodynamic polarisation experiments. The potentiodynamic polarization curves of HDG steel immersed in 0.86 mol.dm^{-3} NaCl with additions of varying BTA concentrations are shown in Figs. 11a and 11b for the anodic and cathodic branches, respectively. Both sets of experiments showed that the open corrosion potential is shifted more positively with increasing BTA concentration, indicative of a net anodic inhibitory effect. The potentiodynamic curves in both Figs. 11a and 11b show that with increasing concentrations of BTA, both anodic and cathodic current density values decrease, indicating that BTA acts as a mixed-type inhibitor.

A comparison of the previous results suggests that BTA is a mixed inhibitor with a predominantly anodic inhibitory effect. In the case of in-coating HT-BTA^-, released BTA^- must migrate to the bare zinc surface within the model defect to cause anodic inhibition. However, with the previous Stratmann type cathodic delamination experiments, the model defect area is large and presumably contains an unrepresentative low concentration BTA^- anions. Therefore, the previous delamination experiments are not anodically limited and give rise to the question as to whether the BTA^- detected within the model defect could significantly contribute to the observed inhibition of cathodic disbondment. Therefore, a series of SKP experiments were carried out where various concentrations of BTA were added to the initiating electrolyte within the model defect. Values for time-dependent E_{corr} vs delamination distance profiles plotted as a function of the square route of time (Fig. 12) showed that the additions of different BTA concentrations to the model defect caused a 7 h delay in the delamination initiation time. Furthermore, in concordance with previous results for HT-BTA^-, delamination rate decreases with increasing BTA concentration, and a deviation to linear delamination kinetics appeared to occur. This suggests that electron transfer is the rate-limiting step. The reduction in the rate of delamination observed is small compared to the case of HT-BTA^- dispersed within the model coating. This result has the implication that anodic inhibition cannot be the main mechanism by which BTA inhibits cathodic disbondment. The delay in the delamination initiation time may be the result of cathodic inhibition within the model defect. Previous research has established that BTA inhibits corrosion via the formation of an adsorbed layer at the cathode, which will, in turn, reduce the rate of the ORR. Such a protective layer inhibiting the cathodic reaction of general corrosion within the model defect could explain a similar length delay in initiation time observed for different concentrations of BTA additions. Once present near the cathodic delamination front, BTA will experience higher pH conditions and undergo deprotonation as described in reaction (2). Hence, it can conceivably be hypothesized that BTA offers predominantly cathodic inhibition by forming an adsorbed layer which reduces rate of the ORR.

Conclusions

Various hydrotalcite-based smart-release corrosion inhibitors containing a range of inorganic and organic anions were added to a PVB coating to determine an effective, environmentally friendly alternative to pigments based upon sparingly soluble hexavalent chromium salts. The majority of the smart release inhibitors led to a reduction in the rate of cathodic disbondment from HDG (summarised in Tables I and II). Still, inhibition efficiency was strongly related to the nature of the anion incorporated within the HT delivery system. Of the inorganic anions evaluated, none performed as well as chromate. However, certain organic anions produced a level of inhibition equivalent to that of chromate.

HT-BTA^- effectively reduced the rate of corrosion and caused a significant delay in the initiation of the cathodic delamination process. This study has identified three main modes by which HT-BTA- inhibits the cathodic disbondment of PVB coatings from HDG. Firstly HT-BTA^- must encounter anionic species (typically Cl^- and OH^- ions in the region of the model defect), at which point the anion will be sequestered and exchanged with BTA^-. This

exchange process, however, has been shown to produce a negligible reduction in the rate of cathodic delamination.

Secondly, HT-BTA is thought to inhibit the cathodic disbondment mechanism by anodic inhibition of the bare zinc surface within the model defect, as demonstrated by potentiodynamic polarisation, SEM and XPS results. These results may be explained by the formation of $Zn(BTA)_{n(s)}$ oligomers or $Zn(BTA)_{2(s)}$ salts at the anode. Prior studies have suggested that BTA reacts with zinc ions produced during the anodic dissolution reaction (5). It has been suggested that either an insoluble precipitate of zinc-benzotriazole salt[109] or a metal-polymeric film is formed.[110]

Lastly, the primary mode of inhibition is thought to be $HT\text{-}BTA^-$ produced cathodic inhibition within the underfilm delaminated zone and critically within the region of the cathodic delamination front as demonstrated by potentiodynamic polarisation experiments, SKP and, most significantly, the SKP study where BTA was added to the initiating electrolyte within the model defect.

Acknowledgments

The authors would like to thank TATA Steel for providing the samples and EPSRC for the funding of the EngD studentships via the Collaborate Training Account (GR/T11333/01). We would also like to acknowledge the assistance provided by Swansea University College of Engineering *AIM* Facility, which was funded in part by the EPSRC (EP/M028267/1), the European Regional Development Fund through the Welsh Government (80708) and the Ser Solar project via Welsh Government. Furthermore, we would like to thank everyone at SPECIFIC IKC which was funded by WEFO (c80892) and EPSRC (EP/N020863/1) for their help support and guidance.

ORCID

P. Ansell https://orcid.org/0000-0002-1797-3015
J. Searle https://orcid.org/0000-0003-1101-075X
N. Wint https://orcid.org/0000-0002-9229-5728

References

1. A. Leng, H. Streckel, and M. Stratmann, *Corros. Sci.*, **41**, 579 (1998).
2. A. Leng, H. Streckel, and M. Stratmann, *Corros. Sci.*, **41**, 547 (1998).
3. A. Leng, H. Streckel, K. Hofmann, and M. Stratmann, *Corros. Sci.*, **41**, 599 (1998).
4. E. L. Koehler, *J. Electrochem. Soc.*, **132**, 1005 (2006).
5. N. W. Khun and G. S. Frankel, *Corros. Sci.*, **67**, 152 (2013).
6. S. J. Caraguay, T. S. Pereira, R. O. Giacomelli, A. Cunha, M. Pereira, and F. A. Xavier, *Surf. Coatings Technol.*, **437**, 128371 (2022).
7. Y. Yin, H. Zhao, M. Prabhakar, and M. Rohwerder, *Corros. Sci.*, **200**, 110252 (2022).
8. W. Fürbeth and M. Stratmann, *Corros. Sci.*, **43**, 229 (2002).
9. W. Fürbeth and M. Stratmann, *Corros. Sci.*, **43**, 229 (2001).
10. C. M. Griffiths, N. Wint, G. Williams, and H. N. McMurray, *Corros. Sci.*, **198**, 110111 (2022).
11. E. L. Koehler, *Corrosion*, **33**, 209 (1977).
12. H. Leidheiser Jr, *Corrosion*, **38**, 374 (1982).
13. H. Leidheiser, W. Wang, and L. Igetoft, *Progress in Organic Coatings*, **11**, 19 (1983).
14. E. L. Koehler, *J. Electrochem. Soc.*, **40**, 1982 (1984).
15. M. Stratmann, H. Streckel, and R. Feser, *Corros. Sci.*, **32**, 467 (1991).
16. M. Stratmann, R. Feser, and A. Leng, *Electrochim. Acta*, **39**, 1207 (1994).
17. G. Williams and H. N. McMurray, *J. Electrochem. Soc.*, **148**, B377 (2001).
18. F. L. Petrilli and S. De Flora, *Appl. Environ. Microbiol.*, **33**, 805 (1977).
19. F. L. Petrilli and S. de Flora, *Mutat. Res. Toxicol.*, **58**, 167 (1978).
20. European Commission, *OJ L*, **396**, 1 (2006).
21. O. Ø. Knudsen and A. Forsgren, "Corrosion control through organic coatings." *Boca Raton : a CRC title, part of the Taylor & Francis,* (Boca Raton, FL)(CRC Press) 2nd ed.p. 276 (2017).
22. O. Gharbi, S. Thomas, C. Smith, and N. Birbilis, *npj Mater. Degrad.*, **2**, 23 (2018).
23. R. Naderi and M. M. Attar, *Dye. Pigment.*, **80**, 349 (2009).
24. J. R. Davis, *Corrosion: Understanding the Basics - Google Books*, **1**, 563 (2000).
25. M. J. Pryor and M. Cohen, *J. Electrochem. Soc.*, **100**, 203 (1953).
26. J. E. O. Mayne, *Br. Corros. J.*, **5**, 106 (1970).
27. A. C. Bastos, M. G. S. Ferreira, and A. M. Simões, *Prog. Org. Coatings*, **52**, 339 (2005).
28. N. Wint, C. M. Griffiths, C. J. Richards, G. Williams, and H. N. McMurray, *Corros. Sci.*, **174**, 108 (2020).
29. V. I. Pokhmurs'kyi, I. M. Zin, S. B. Layon, and L. M. Bilyi, *Mater. Sci.*, **39**, 153 (2003).
30. D. R. Lide, *Handbook of Chemistry and Physics* (Boca Raton, FL)(CRC Press) 89th ed.p. 8.
31. G. A. Blengini et al., *Study on the EU's list of Critical Raw Materials (2020) Final Report*, 1Publications Office of the European Union (2020)2.
32. M. F. Montemor, *Surf. Coatings Technol.*, **258**, 17 (2014).
33. A. Ouarga, N. Lebaz, M. Tarhini, H. Noukrati, H. Noukrati, A. Barroug, A. Elaissari, and H. B. Youcef, *J. Mol. Liq.*, **354**, 118862 (2022).
34. D. A. Leal, A. Kuznetsova, G. M. Silva, J. Tedim, F. Wypych, and C. E. B. Marino, *Appl. Clay Sci.*, **225**, 1 (2022).
35. S. Chen, Z. Huang, M. Yaun, G. Huang, H. Guo, G. Meng, Z. Feng, and P. Zhang, *J. Mater. Sci. Technol.*, **125**, 67 (2022).
36. Y. Cao, D. Zheng, F. Zhang, J. Pan, and C. Lin, *J. Mater. Sci. Technol.*, **102**, 232 (2022).
37. D. G. Evans and X. Duan, *Chem. Commun.*, 485 (2006).
38. D. Nguyen Thuy, H. T. Thi Xuan, A. Nicolay, Y. Paint, and M. G. Olivier, *Prog. Org. Coatings*, **101**, 331 (2016).
39. R. G. Buchheit, H. Guan, S. Mahajanam, and F. Wong, *Prog. Org. Coatings*, **47**, 174 (2003).
40. N. Granizo, J. M. Vega, I. Díaz, B. Chico, D. de la Fuente, and M. Morcillo, *Prog. Org. Coatings*, **70**, 394 (2011).
41. R. G. Buchheit, H. Guan, S. Mahajanam, and F. Wong, *Prog. Org. Coat.*, **47**, 174 (2003).
42. G. Williams and H. N. McMurray, *Electrochem. Solid-State Lett.*, **6**, B9 (2003).
43. G. Williams and H. N. McMurray, *Electrochim. Acta*, **69**, 287 (2012).
44. G. Williams and H. N. McMurray, *Electrochem. Solid-State Lett.*, **7**, B13 (2004).
45. D. E. L. Vieira, A. N. Salak, M. G. S. Ferreira, J. M. Vieira, and C. M. A. Brett, *Appl. Surf. Sci.*, **573**, 21 (2022).
46. T. T. X. Hang, T. A. Truc, N. T. Duong, P. G. Vu, and T. Hoang, *Appl. Clay Sci.*, **67–68**, 18 (2012).
47. E. Alibakhshi, E. Ghasemi, M. Mahdavian, and B. Ramezanzadeh, *Corros. Sci.*, **115**, 159 (2017).
48. Y. Tian, C. Dong, G. Wang, X. Cheng, and X. Li, *Mater. Lett.*, **236**, 517 (2019).
49. S. J. Mills, A. G. Christy, J.-M. R. Génin, T. Kameda, and F. Colombo, *Mineral. Mag.*, **76**, 1289 (2012).
50. S. Miyata, *Clay Clay Miner.*, **31**, 305 (1983).
51. J. Pérez-Ramírez, S. Abelló, and N. M. Van Der Pers, *Chem. - A Eur. J.*, **13**, 870 (2007).
52. B. Chico, J. Simancas, J. M. Vega, N. Granizo, I. Díaz, D. de la Fuente, and M. Morcillo, *Prog. Org. Coatings*, **61**, 283 (2008).
53. D. T. Nguyen, H. T. X. To, J. Gervasi, Y. Paint, M. Gonon, and M. Olivier, *Prog. Org. Coatings*, **124**, 256 (2018).
54. J. M. Vega, N. Granizo, D. De La Fuente, J. Simancas, and M. Morcillo, *Prog. Org. Coatings*, **70**, 213 (2011).
55. V. Shkirskiy, P. Keil, H. Hintze-Bruening, F. Leroux, P. Vialat, K. Ogle, and P. Volovitch, *ACS Appl. Mater. Interfaces*, **7**, 25180 (2015).
56. I. M. Zin, V. I. Pokhmurskii, J. D. Scantlebury, and S. B. Lyon, *J. Electrochem. Soc.*, **148**, B293 (2001).
57. Y. Hao, F. Liu, E. H. Han, S. Anjum, and G. Xu, *Corros. Sci.*, **69**, 77 (2013).
58. F. Cavani, F. Trifiro, and A. Vaccari, *Catal. Today*, **11**, 173 (1991).
59. G. Williams, S. Geary, and H. N. McMurray, *Corros. Sci.*, **57**, 139 (2012).
60. M. Stratmann and H. Streckel, *Corros. Sci.*, **30**, 681 (1990).
61. M. Stratmann, A. Leng, W. Fürbeth, H. Streckel, H. Gehmecker, and K. H. Große-Brinkhaus, *Prog. Org. Coatings*, **27**, 261 (1996).
62. H. N. Mcmurray and G. Williams, *Shreir's Corrosion*, **4**, 988 (2010).
63. C. F. Glover, R. Subramanian, and G. Williams, *J. Electrochem. Soc.*, **162**, C433 (2015).
64. N. Wint, P. Ansell, J. Edy, G. Williams, and H. N. McMurray, *J. Electrochem. Soc.*, **166**, C580 (2019).
65. H. N. McMurray and G. Williams, *Ref. Modul. Mater. Sci. Mater. Eng.*, **1**, 1 (2016).
66. M.-W. Huang, C. Allely, K. Ogle, and M. E. Orazem, *J. Electrochem. Soc.*, **155**, C279 (2008).
67. G. Williams and H. N. McMurray, *Prog. Org. Coatings*, **102**, 18 (2017).
68. G. Williams, H. N. McMurray, and D. A. Worsley, *J. Electrochem. Soc.*, **149**, L4 (2002).
69. D. Wang, X. Tang, Y. Qiu, F. Gan, and G. Zheng Chen, *Corros. Sci.*, **47**, 2157 (2005).
70. M. S. Vukasovich and J. P. G. Farr, *Mater. Perform.*, **25**, 9 (1986).
71. V. Shkirskiy, P. Keil, H. Hintze-Bruening, F. Leroux, T. Stimpfling, D. Dragoe, K. Ogle, and P. Volovitch, *Corros. Sci.*, **99**, 31 (2015).
72. S. Morsch, S. Emad, L. Farren, M. D. Goodall, S. B. Lyon, and S. R. Gibbon, *Sci Rep.*, **8**, 17450 (2018).
73. T. S. N. Sankara Narayanan, *Rev. Adv. Mater. Sci.*, **9**, 130 (2005).
74. R. Romagnoli and V. F. Vetere, *Corros. Rev.*, **13**, 45 (1995).
75. N. Van Phuong, K. Lee, D. Chang, M. Kim, S. Lee, and S. Moon, *Met. Mater. Int.*, **19**, 273 (2013).
76. H. Sheng, C. F. Dong, K. Xiao, X. G. Li, and L. Lu, *Int. J. Miner. Metall. Mater.*, **19**, 939 (2012).
77. C. F. Glover, C. A. J. Richards, G. Williams, and H. N. McMurray, *Corros. Sci.*, **136**, 304 (2018).
78. R. J. Holness, G. Williams, D. A. Worsley, and H. N. McMurray, *J. Electrochem. Soc.*, **152**(2), 1 (2005).
79. M. Pourbaix, H. Zhang, and A. Pourbaix, *Mater. Sci. Forum*, **251**, 143 (1997).
80. V. Rives, M. del Arco, and C. Martín, *Appl. Clay Sci.*, **88**, 239 (2014).
81. Y. Wang and D. Zhang, *Mater. Res. Bull.*, **46**, 1963 (2011).
82. N. Aware and K. Hirlekar, *J. Sci. Ind. Res. (India).*, **68**, 267 (2016).

83. E. V. Bendinelli, I. V. Aoki, O. Barcia, and I. C. P. Margarit-Mattos, *Mater. Chem. Phys.*, **238**, 121883 (2019).
84. M. L. Zheludkevich, K. A. Yasakau, S. K. Poznyak, and M. G. S. Ferreira, *Corros. Sci.*, **47**, 3368 (2005).
85. M. Muniz-Miranda, F. Muniz-Miranda, and S. Caporali, *Beilstein J. Nanotechnol.*, **5**, 2489 (2014).
86. B. El Ibrahimi, A. Soumoue, A. Jmiai, H. Bourzi, R. Oukhrib, K. E. Mouaden, S. E. Issami, and L. Bazzi, *J. Mol. Struct.*, **1125**, 93 (2016).
87. K. Babić-Samardžija and N. Hackerman, *J. Solid State Electrochem.*, **9**, 483 (2005).
88. M. Andersson Trojer, A. Movahedi, H. Blanck, and M. Nydén, *J. Chem.*, **2013**, 946 (2013).
89. L. D. Freedman and G. O. Doak, *Chem. Rev.*, **57**, 479 (1957).
90. K. Aramaki, *Corros. Sci.*, **43**, 2201 (2001).
91. L. Feng, Y. Zhiyong, Q. Zhouhaia, L. Guomingc, L. Zhcnhua, and Z. Daquan, *Corros. Prot.*, **40**, 28 (2019).
92. M. Kalinowska, R. Świsłocka, and W. Lewandowski, *J. Mol. Struct.*, **993**, 404 (2011).
93. S. M. N. Mohsin et al., *Chem. Cent. J.*, **7**, 7 (2013).
94. P. T. Gilbert and S. E. Hadden, *J. Appl. Chem.*, **3**, 545 (2007).
95. T. B. Rawal, M. D. Smith, A. Ozcan, J. C. Smith, L. Tetard, S. Santra, and L. Petridis, *ACS Appl. Nano Mater.*, **3**, 9951 (2020).
96. S. Kuznetsova, E. Mongush, and K. Lisitsa, *J. Phys. Conf. Ser.*, **1145**, 012020 (2019).
97. K. Ikeda and H. Takeda, *Chem. Pharm. Bull.*, **12**, 303 (1964).
98. Z. Maskos, J. D. Rush, and W. H. Koppenol, *Arch. Biochem. Biophys.*, **296**, 521 (1992).
99. Z. Maskos, J. D. Rush, and W. H. Koppenol, *Free Radic. Biol. Med.*, **8**, 153 (1990).
100. A. M. Chiorcea-Paquim, T. A. Enache, E. De Souza Gil, and A. M. Oliveira-Brett, *Compr. Rev. Food Sci. Food Saf.*, **19**, 1680 (2020).
101. P. A. Sørensen, C. E. Weinell, K. Dam-Johansen, and S. Kiil, *J. Coatings Technol. Res.*, **7**, 773 (2010).
102. X. Yang, J. Kirsch, Y. Zhang, J. Fergus, and A. Simonian, *J. Electrochem. Soc.*, **161**, E3036 (2014).
103. T. Adrian Enache, O. Fatibello-Filho, and A. Maria Oliveira-Brett, *Comb. Chem. High Throughput Screen.*, **13**, 569 (2012).
104. C. de, L. Ribeiro, J. G. M. Santos, J. R. de Souza, M. A. Pereira-da-Silva, and L. G. Paterno, *J. Electroanal. Chem.*, **805**, 53 (2017).
105. G. Mengoli, M. M. Musiani, E. Preparativa, and C. S. Uniti, *J. Electrochem. Soc.*, **134**, 643 (1987).
106. C. A. J. Richards, H. N. McMurray, and G. Williams, *Corros. Sci.*, **154**, 101 (2019).
107. G. Williams, H. N. McMurray, and M. J. Loveridge, *Electrochim. Acta*, **55**, 1740 (2010).
108. J.-L. Wang, C. Ke, K. Pohl, N. Birbilis, and X.-B. Chen, *J. Electrochem. Soc.*, **162**, C403 (2015).
109. V. Sirtori, F. Zambon, and L. Lombardi, *J. Electron. Mater.*, **29**, 463 (2000).
110. A. M. Fenelon and C. B. Breslin, *J. Appl. Electrochem.*, **31**, 509 (2001).